7547

THE EVAPORATION OF AN IRON - 5 AND 25 PERCENT CHROMIUM ALLOY

THE EVAPORATION OF AN IRON - 5 PERCENT AND AN IRON - 25 PERCENT CHROMIUM ALLOY IN THE TEMPERATURE RANGE 900°C to 1080°C.

By

LARRY ARTHUR MORRIS, B.A.

A Thesis

Submitted to the Faculty of Graduate Studies

in Partial Fulfilment of the Requirements

for the Degree

Master of Science

McMaster University

October, 1962

MASTER OF SCIENCE (1962) McMASTER UNIVERSITY
(Metallurgy) Hamilton, Ontario

TITLE: The evaporation of an Iron - 5 Percent and an Iron - 25 Percent Chromium Alloy in the Temperature Range 900°C to 1080°C.

AUTHOR: Larry Arthur Morris, B.A. (McMaster University)

SUPERVISOR: Professor W.W. Smeltzer

NUMBER OF PAGES: ix, 104

SCOPE AND CONTENTS:

In this thesis, the theory of metal crystal evaporation and of vapour pressure determinations are presented, followed by a literature survey on the evaporation characteristics of iron, chromium and alloys of iron - chromium. Results are presented for an investigation carried out on the free evaporation kinetics of iron base alloys containing 5 percent and 25 percent chromium for the temperature range 900°C to 1080°C. Also, a complete description of the surface topographies of evaporated specimens is presented using normal, hot stage and interferometric microscopic techniques. These results are correlated in terms of the evaporation theory and pertinent experimental data reported for other metallic systems.

ACKNOWLEDGEMENTS

The author sincerely appreciates the interest and guidance demonstrated by his research director, Dr. W.W. Smeltzer, throughout all phases of this project.

The author would also like to express his gratitude to the Faculty and graduate students of the Department of Metallurgy and Metallurgical Engineering for their suggestions and many helpful discussions, to Mr. W.E. Boggs of the United States Steel Corporation, Applied Research Laboratory, Monroeville, Pa., who kindly supplied the alloys used in this investigation, and to Mr. J.H. Kelly of the Steel Co. of Canada, Spectrographic Laboratory, Hamilton, Ontario, who supplied the author with a detailed analysis of the alloys.

This project was supported by grants from the U.S. Air Force Office of Scientific Research, Air Research and Development Command, and the Defence Research Board, Ottawa, Canada, to Dr. W.W. Smeltzer.

The hot stage assembly used in this investigation was designed and constructed by G.R. Purdy, Department of Metallurgy and Metallurgical Engineering, McMaster University, Hamilton, Ontario.

TABLE OF CONTENTS

LIST OF ILLUSTRATIONS

LIST OF TABLES

CHAPTER I

INTRODUCTION

As technology is advanced, the need for materials is increasingly demanded, capable of withstanding various atmospheres at elevated temperatures. Two common environments, encountered at elevated temperatures are; those which promote external oxide scale formation, and those which promote evaporation.

Many experiments have been performed in order to determine the oxidation characteristics of most metals and alloys. Of the metals and alloys considered, iron and alloys of iron, namely iron - chromium, iron - nickel and iron - chromium - nickel alloys, have been widely investigated. Investigations on the system iron - chromium, with chromium contents below 12 percent, have yielded non reproducible rate data and abnormal surface features (1) as a result of the type of oxide films formed on these alloys. With chromium contents greater than 12 percent, the results of experimental investigations appear to be reproducible within the limits of experimental error.

The evaporation kinetics of the metals iron and chromium have been established with suitable accuracy; however, the kinetics of evaporation of the system iron - chromium are still not well defined. In all investigations,

only the weight loss measurements and pertinent thermodynamic data have been reported. The effect of evaporation on surface topography, and visa versa, is relatively poorly understood.

In this thesis, the results of evaporation experiments are reported for an iron - 5 percent and an iron - 25 percent chromium alloy in the temperature range 900°C to 1080°C. The vapour pressures, determined from weight loss measurements under conditions of free evaporation, are compared to those calculated from existing thermodynamic data, assuming the system iron - chromium to behave ideally. The condensation coefficient, α, determined from the ratio of the observed pressure to the ideal pressure, is reported for all temperatures considered. A complete description of surface topography is included and the effect of thermal etching on evaporation is discussed in terms of the theory of metal crystal evaporation.

CHAPTER II

THEORETICAL CONSIDERATIONS

2.1 Theoritical Analysis of the Determination of the Vapour Pressures of Pure Metals

2.1 (i) Introduction

The methods used for the determination of the vapour pressures of metals can be divided into two classifications depending upon the magnitudes of the pressures being measured. High pressure methods are employed when the vapour pressure is in the pressure range of 10^{-2} to 10^{-3}mm. Hg, and low pressure methods when the pressures are in the range 10^{-2} to 10^{-9}mm. Hg. High pressure methods can again be categorized into static methods, (manometric, boiling point, weighing, dew point, vapour concentration and density methods) and dynamic methods, the principal one being the gas entrainment method. The principles of these methods will not be discussed here since the vapour pressure measurements, to be described later, do not lie in the high pressure range. The reader is referred to a monograph by Speiser and Spretnak [2] for a review of this subject.

In the low pressure range, dynamic methods, involving measurements of evaporation and effusion rates, have been extensively used to determine the vapour pressures of metals. The usage of these methods arises from two causes:

(a) the rates of evaporation and effusion of material

from the condensed phase to the vapour phase are directly proportional to time. Consequently, a material with a low vapour pressure may be evaporated over long time periods allowing one to obtain accurate measurements for the rate of material loss from which the vapour pressure may be calculated.

(b) high pressure methods cannot be employed for investigations of materials, for example, involatile refractory metals, which react with their environment at temperatures sufficiently high for accurate measurement of pressure. The application of low pressure methods allows measurements at lower temperatures under high vacuum conditions which greatly refine experimental technique.

2.1 (ii) Free Evaporation Method for the Determination of the Vapour Pressures of Metals

Langmuir [3] devised a dynamic method, based upon the kinetic-molecular theory of gases, to determine the vapour pressures of refractory metals from their weight loss when heated in a vacuum.

If a solid is in a state of equilibrium with its vapour, we then regard this equilibrium as a balance between the rates of evaporation and condensation. That is, the number of atoms which evaporate from the surface is equal to the number of atoms which condense on the surface per unit time. The number of evaporating atoms depends upon their number at the surface having sufficient thermal energy to escape the attractive forces of their neighboring atoms, and

also, upon the external pressure. At temperatures where the vapour pressure of a substance does not exceed a millimeter, one may generally neglect the effect of molecular collisions in the vapour phase on evaporation rates. Hence, the rate of evaporation is the same in a vacuum as in the presence of saturated vapour. The rate of condensation, however, only depends on the vapour pressure. It can therefore be seen that;

vapour pressure~rate of condensation = rate of evaporation (1)

The rate at which atoms from the vapour phase collide with the surface can be calculated from the kinetic-molecular theory of gases. The mass, m, of vapour atoms striking unit area per unit time is,

$$m = \tfrac{1}{4} \rho \bar{v} \qquad (2)$$

where ρ is the density of the vapour and $\bar{v}$ is the mean molecular average velocity.

From the ideal gas equation,

$$\rho = \frac{pM}{RT} \qquad (3)$$

where p is the pressure, M is the molecular weight of the vapour, R is the gas constant, and T is the absolute temperature. Substituting (3) into (2), and, noting that,

$$\bar{v} = \sqrt{\frac{8RT}{\pi M}} \qquad (4)$$

we find,

$$p = m \sqrt{\frac{2\pi RT}{M}} \qquad (5)$$

This result is based upon the assumption that every atom which strikes the surface condenses. Accordingly, equation (5) gives the desired relation between the vapour pressure and the rate of evaporation in a vacuum. However, it could be equally well assumed that only a fraction, α, of the atoms, colliding with the surface, condense. The vapour pressure should then be calculated from a modified expression for equation (5), namely,

$$p = \frac{m}{\alpha}\sqrt{\frac{2\pi RT}{M}} \qquad (6)$$

The correction factor, α, is designated the condensation coefficient. Therefore, vapour pressures of substances can be computed by means of (6) if the value of this coefficient can be evaluated. For metallic systems, investigators have determined or assumed $\alpha \simeq 1$. The properties of the condensation coefficient will be discussed more fully in section 2.3.

2.1 (iii) Effusion Method for the Determination of the Vapour Pressures of Metals

Knudsen [4] devised a method for the determination of vapour pressures of condensed phases by considering the effusion rate of a vapour through a small orifice separating the region where the vapour is in equilibrium with the condensate from a region of high vacuum. This method differs in principle from the Langmuir technique only in that an opening is provided through which the vapour escapes rather than having it escape from the surface of the material itself. For the

application of this technique, Knudsen [5] has shown that the pressure must be sufficiently low so that the ratio of the mean free path of the atoms in the vapour to the diameter of the orifice is greater than 10. If this condition is satisfied, the effusion rate through an orifice of negligible wall thickness will depend only on the difference in pressure across the orifice (the pressure difference between the Knudsen cell and the vacuum chamber), the orifice diameter and the gas density. If the pressure, p, inside the Knudsen cell is assumed to be the equilibrium pressure, it can be shown that the relation between this pressure and the effusion rate is,

$$p = m\sqrt{\frac{2\pi RT}{M}} \qquad (7)$$

It can immediately be seen that this relation is identical to (6) with the exception of the condensation coefficient, α. Since the determination of the vapour pressure by this method depends only on the amount of material which has effused through the orifice, the Knudsen technique permits an unambiguous determination of vapour pressures for solids and liquids. However, there is one serious disadvantage in the utilization of this technique. The quantity of material which effuses through the small orifice may be so minute that an accurate evaluation may not be made of the weight loss m. On the other hand, the Langmuir method can be employed to measure vapour pressures that are a factor of 10^{-3} to 10^{-4} smaller. Here, the larger weight loss from the larger area

of the freely evaporating surface permits a higher degree of accuracy in measuring the evaporation rates.

The Knudsen cell must be constructed according to rigorous specifications. The geometry of the orifice in the cell is subject to two restrictions, namely, the diameter and the length of the orifice wall. The maximum allowable orifice area is governed by the effect of effusion on the vapour pressure in the cell. If no hole is present, a pressure p', the true vapour pressure at some temperature, will be established. However, if an orifice of area h is introduced, a steady state value of the pressure p, will occur where $p < p'$. This steady state value of the pressure is attained when the effusion rate through the orifice is equal to the evaporation rate from the effective area, s, within the cell (the inside diameter of the cell). Speiser and Spretnak [2] have shown that the relation between the true vapour pressure p' and the steady state pressure, p, is,

$$p = p' \frac{\alpha}{h/s + \alpha} \qquad (8)$$

Here, h and s are the orifice area and cross-sectional area of the cell respectively. Thus, if $h/s << \alpha$, then $p \approx p'$.

The second factor to be considered is that of orifice wall length. The process must be considered as effusion through a short tube if the walls have appreciable length. Molecular collisions with the walls of the tube reduce the rate of effusion and, hence, lead to an inaccurate determination of the

vapour pressure. Clausing [6] has made a detailed study of this problem, and Kennard [7] devised empirical relations which reproduce the corrections, deduced by Clausing, with good agreement. Thus, a correction factor, K, appears in the Knudsen equation,

$$p = \frac{m}{K}\sqrt{\frac{2\pi RT}{M}} \qquad (9)$$

where $K = \frac{1}{1 + 0.5\ 1/a}$, for $0 \leq 1/a \leq 1.5$ (10)

and $K = \frac{1 + 0.4\ 1/a}{1 + 0.95\ 1/a + 0.15\ (1/a)^2}$, for $1/a > 1.5$ (11)

Here, l is the wall length of the orifice and a is the radius. Despite these limitations, experimenters generally may construct the Knudsen cell so that $K \approx 1$. Knudsen's equation (7) may then be employed for determinations of vapour pressures.

2.2 Theoretical Aspects of the Determination of the Vapour Pressures of Alloys

2.2 (i) Introduction

The vapour pressures of components in alloy systems are not only of intrinsic value, but also provide data from which chemical activities and heats of solution can be calculated for liquid and solid alloy systems. The vapour pressure method is especially convenient when the system is chemically reactive. Also, this method may be applicable to cases where the determination of thermodynamic properties by electromotive cell measurements fail due to polarization and

diffusion effects in solids.

2.2 (ii) Free Evaporation and Effusion Methods for the Determination of Vapour Pressures of Alloys

There are no essential differences in the determinations of vapour pressure relations for alloy systems compared to those for pure metals, if the condensation coefficient is of a value equal to one. For this condition, the methods mentioned in section 2.1 (i) and the principles employed in deriving the expressions for the rates of evaporation and effusion are identical. These methods, however, only permit the direct measurement of the total vapour pressures, and do not allow a direct determination of the partial pressures of the alloying constituents in the vapour phase. These partial pressures can only be determined if the vapour is collected and analyzed for composition. For metallic vapour, the partial pressures may then be generally calculated by employing Dalton's Law for Partial Pressures. Subsequently, the activities of the components can be estimated. In some cases, due to difficulties encountered in collecting the vapour, only the total pressure can be obtained. Where such systems show nearly ideal behaviour, the activity coefficients have been estimated by invoking the concept of regular solution behaviour.[8] The molecular weights of the evaporating species must be known in order to calculate the vapour pressures over alloys in both the evaporation and effusion methods.

2.3 The Condensation Coefficient

The condensation coefficient, α, has been defined as the fraction of colliding atoms or molecules, in equilibrium with a solid, which condense upon impact with the surface. Therefore, a fraction, $(1 - \alpha)$, of the atoms is reflected from the surface. As was shown in section 2.1 (ii), α, is a coefficient which must be known or ascertained in order to use the Langmuir method for the determination of vapour pressures. Consequently, many investigators[2,8,9] employing various techniques, have determined α for different systems. For metallic systems, the experimental results show that $\alpha \approx 1$.[8,10,11,12,13]

It has been reported that this coefficient is also less than unity presumably due to impurity adsorption or oxide contamination of metallic surfaces. Recently, Hirth and Pound [15,16] have questioned this viewpoint, and carried out a detailed theoretical analysis of the mechanism of crystal evaporation. Their analysis demonstrated that the condensation coefficient is a function of both the vapour pressure and temperature. They found that α, for a perfectly clean metallic surface, can vary from 1/3 to 1. Experiments were then carried out on the evaporation rate of single silver crystals to test this theoretical prediction. They demonstrated that these evaporation results suitably agreed with the theoretical predictions for the evaluation of the condensation coefficient.

The properties of α will be further amplified in the

following sections.

2.4 Theory of Metal Evaporation

2.4 (i) Introduction

The purpose of the following sections is to illustrate that an atomistic model of a metal crystal, in conjunction with a mechanism of surface diffusion and desorption, can be used to predict and correlate phenomena expected in connection with the vaporization process. It will be shown that the relation for the condensation coefficient, α, is a function of temperature and pressure for a pure metal exhibiting a monatomic vapour.

2.4 (ii) Review of Evaporation Theory

The concepts of evaporation have been developed in several distinct stages. The first dealt with the problem of how long it would take an atom or molecule to leave its potential trough at the surface, where it is bound by the energy of evaporation, λ. Polanyi, Wigner [17] and Neumann [18] solved this problem by statistical methods and presented equations for evaporation rates. In this development, it was necessary to assume that all the surface atoms possessed a binding energy λ, and that each had an equal opportunity to evaporate. This assumption, however, is not valid for crystalline solids since most of the molecules are bound by an energy greater than λ, as was shown by Kossel.[19] As a result, Volmer[20] introduced the second stage of development of crystal evaporation theory by his concept of stepwise evaporation. According

to Volmer atoms are able to leave their "half crystal positions", where they are bound with an energy equal to the energy of evaporation, and move to the surface. At this position, they are less strongly bound and only adsorbed. Hence, these atoms may migrate on the surface by surface diffusion for various time intervals until evaporation takes place. Thus, theory was now based upon the concepts of surface diffusion and crystal imperfections.

More recently, Volmer's ideas have been formulated quantitatively by Burton, Cabrera, Frank[21,22] and Knacke, Stranski and Wolff[23,24] to obtain equations for the evaporation rate of crystals.

2.4 (iii) Mechanism of Metal Evaporation

The concept of stepwise evaporation, that is, that evaporation takes place by means of an adsorbed layer, is a direct consequence of the theoretical and experimental works of Langmuir, Knudsen and Volmer.

Langmuir [25] demonstrated that as an atom approaches the solid surface, it is attracted, and thus gains additional kinetic energy. When it strikes the surface, only a few adjacent atoms are affected, since the energy is very rapidly dissipated into the crystal. He concluded that there were no elastic reflections and only a process of condensation and re-evaporation. Consequently, the condensation coefficient would be unity.

Knudsen [26] stated that the reflection of vapour from

the surface must be diffuse, where the angle of reflection does not depend on the angle of incidence. Specifically, the evaporation probability normal to the surface should show a cosine distribution. He showed by experiment, that this indeed was the case. These concepts may be explained on the basis of an adsorbed layer.

Volmer [27] then observed that Hg crystals grow laterally at a rate 1,000 times faster than expected for an immobile adsorbed layer of atoms. These observations could only be rationalized by assuming that the atoms in the adsorbed layer exhibited an appreciable mobility.

It might be mentioned here that no all embracing theory exists regarding condensation and evaporation. However, Knacke and Stranski [9] have summarized theoretical approaches to the mechanism of evaporation. They show that evaporation involves escape from regular lattice positions to edges, corners, and monatomic steps on the crystal surface, then to adsorbed positions and finally to the vapour. This basic mechanism is an essential feature of the theory for evaporation of metal crystals. There is justification for this viewpoint. Burton, Cabrera and Frank [21] have shown that the converse process of crystal growth from the vapour proceeds by adsorption, surface diffusion to the edge of an advancing monolayer, and then diffusion along the edge to a kink or half crystal position. The ledges mentioned arise from screw dislocations, stepped monolayers, or other nonequilibrium imperfections.

At this point, it is necessary to introduce a model of a crystal surface after Kossel [19] and Stranski [28,29], as is shown in Figure 1. Several characteristic atom positions are identified in this figure: (a) in a surface, (b) in a ledge, (c) at a kink, (d) at a ledge and (e) adsorbed on the surface. The reader may notice that the kink or half crystal position constitutes the starting point in stepwise evaporation (growth site in condensation). An atom or molecule leaving the kink position gives rise to the repeatable step in stepwise evaporation.

Employing the nomenclature of Hirth and Pound [15], the state of the surface during evaporation can be described by the following relations :

$$\text{atoms in ledge} \rightleftharpoons \text{atoms in kinks} \tag{12}$$

$$\text{atoms in kinks} \rightleftharpoons \text{atoms at ledge} \tag{13}$$

$$\text{atoms at ledge} \underset{r_2}{\overset{r_1}{\rightleftharpoons}} \text{adsorbed atoms} \tag{14}$$

$$\text{adsorbed atoms} \underset{r_4}{\overset{r_3}{\rightleftharpoons}} \text{atoms in vapor} \tag{15}$$

$$\text{atoms at ledge} \underset{r_6}{\overset{r_5}{\rightleftharpoons}} \text{atoms in vapour} \tag{16}$$

where the r's represent the rates of the reactions considered and are in units of number of atoms per cm^2 of surface per second. These rates, at equilibrium may be written as:

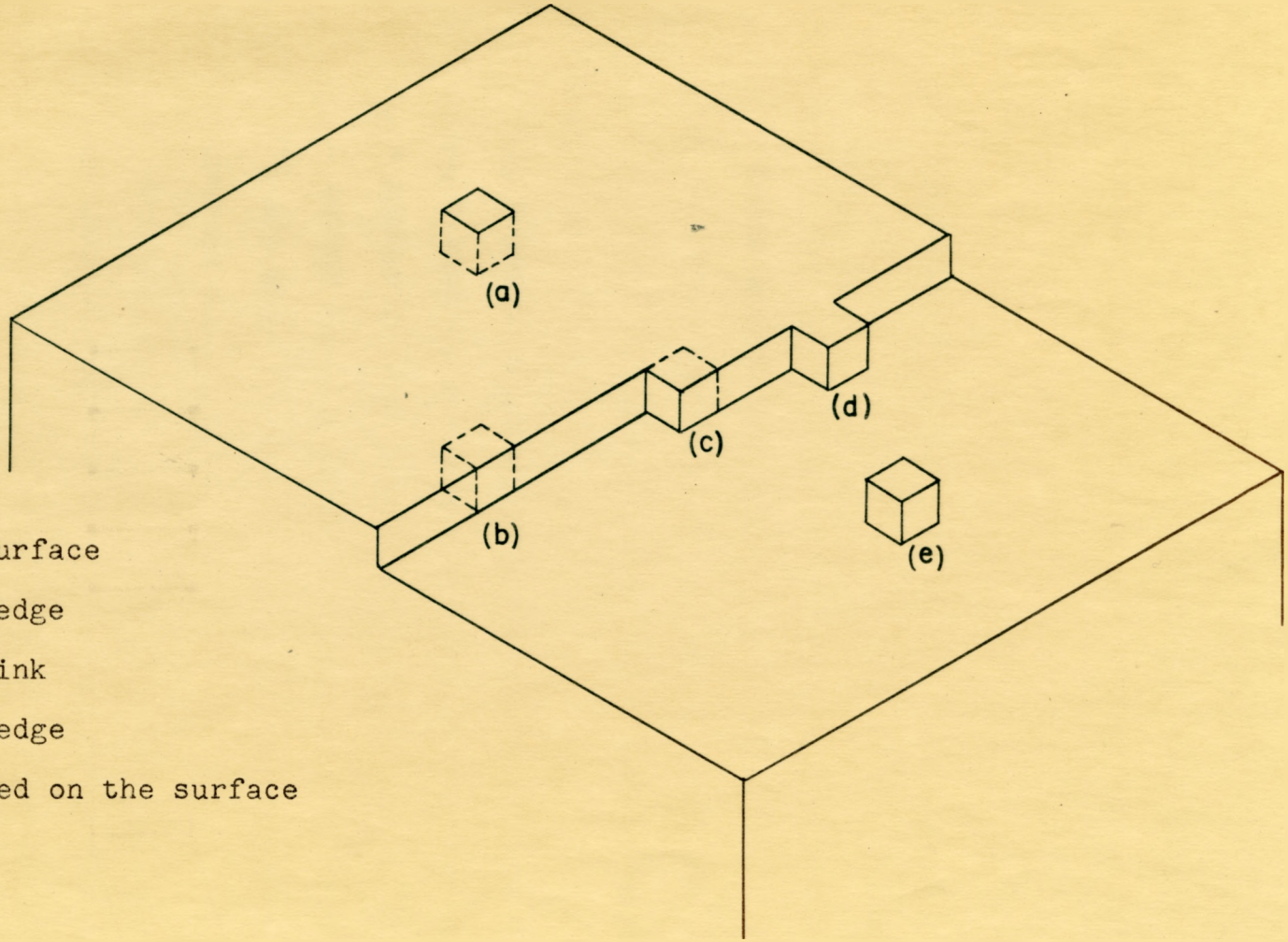

(a) in a surface

(b) in a ledge

(c) at a kink

(d) at a ledge

(e) adsorbed on the surface

Figure 1. Model of a crystal surface illustrating characteristic atom positions

$$r_1 = y.\ n\ (L)_e\ \nu \exp(-\Delta F_1/kT) \qquad (17)$$

$$r_2 = 2y\gamma.n(s)_e\ \nu \exp(-\Delta F_D/kT) \qquad (18)$$

$$r_3 = n(s)_e \nu \exp(-\Delta F_3/kT) \qquad (19)$$

$$r_4 = P_e / (2\pi mkT)^{\frac{1}{2}} \qquad (20)$$

$$r_5 = y.n(L)_e \nu \exp(-\Delta F_5/kT) \qquad (21)$$

$$r_6 = (yn_y/n_o)\ .\ P_e / (2\pi mkT)^{\frac{1}{2}} \qquad (22)$$

where y = ledge length per cm^2,

ν = vibration frequency of atoms at the surface,

γ = probability of a given jump direction in random walk of atoms on the surface,

$n(s)_e$ = equilibrium concentration of adsorbed atoms,

$n(L)_e$ = equilibrium concentration of atoms at a ledge,

n_y = number of atom sites per unit length of ledge,

n_o = number of atom sites per unit area of surface,

and the ΔF's are the free energies of activation for the particular process considered.

One consequence of this system of equations lies in the fact that they may be used to gain some insight concerning the assumption previously made about the mechanism of stepwise evaporation. Basically it is necessary to analyse the two principal processes, namely, (a) dissociation of atoms at ledge positions (r_1), and subsequently desorption (r_3) or (b) by direct evaporation from positions at a ledge (r_5). In order

to determine the correct method by employing equations (17) to (22), it is necessary to know the approximate values of the free energy quantities.

These free energies are estimated by considering the net number of bonds broken for various atom transitions on the surface where only the nearest and next nearest neighbour interactions are utilized. As an approximation for these values, Hirth and Pound [15] evaluated the enthalpy change for each reaction. These energies are good approximations to the values of the free energies because the entropy contributions are relatively small. Table I shows the relation between the Δ F terms and the binding energies involved for various atom transfers. The symbol ϕ and ϕ' represent the binding energies due to nearest and next nearest neighbour interactions respectively. These are further assumed to be additive. Hence, the above equations may be used to estimate which processes occur more readily, and to establish the validity of either process (a), or (b), or both.

We can see that since $F_5 > F_3$ and $n(s) > y.n(L)_e$, $r_3 >> r_5$. Alternatively, since at equilibrium, $r_1 = r_2$, $r_3 = r_4$, $r_5 = r_6$, and $n_o >> yn_y$, then $r_4 >> r_6$ and $r_3 >> r_5$. Also, $\Delta F_5 > \Delta F_1$, and $r_1 >> r_5$. Hence, we may conclude that evaporation occurs by a mechanism of dissociation of atoms from ledges to adsorbed positions and subsequently, to the vapour phase.

TABLE I

FREE ENERGIES OF ACTIVATION FOR VARIOUS ATOM MOVEMENTS

Position change		Kink to at ledge	At ledge to adsorbed	Adsorbed to vapour	At ledge to vapour	Surface diffusion	To form kink in ledge	Kink to Vapour	Vapour from in surface
ΔF of activation		ΔF_0	ΔF_1	ΔF_3	ΔF_5	ΔF_D	ΔF_7	ΔF_9	ΔF_{10}
Lattice	Plane								
fcc	(111)	ϕ	2ϕ	$3\phi + 3\phi'$	$5\phi + 3\phi'$	$< \phi$	$\phi/2$	$6\phi + 3\phi'$	$9\phi + 3\phi'$
fcc	(100)	ϕ'	$2\phi + \phi'$	$4\phi + \phi'$	$6\phi + 2\phi'$	$< \phi$	$\phi'/2$	$6\phi + 3\phi'$	$8\phi + 5\phi'$
bcc	(100)	ϕ'	ϕ'	$4\phi + \phi'$	$4\phi + 2\phi'$	$< \phi$	$\phi'/2$	$4\phi + 3\phi'$	$4\phi + 5\phi'$
bcc	(110)	ϕ'	2ϕ	$2\phi + 2\phi'$	$4\phi + 2\phi'$	$< \phi$	$\phi'/2$	$4\phi + 3\phi'$	$6\phi + 4\phi'$
Simple cubic	(100)	ϕ	$\phi + 2\phi'$	$\phi + 4\phi'$	$2\phi + 6\phi'$	$< \phi$	$\phi/2$	$3\phi + 6\phi'$	$5\phi + 8\phi'$
Simple cubic	(110)	ϕ'	ϕ	$2\phi + 5\phi'$	$3\phi + 5\phi'$	$< \phi$	$\phi/2$	$3\phi + 6\phi'$	$4\phi + 7\phi'$
hcp	(0001)	ϕ	2ϕ	$3\phi + 3\phi'$	$5\phi + 3\phi'$	$< \phi$	$\phi/2$	$6\phi + 3\phi'$	$9\phi + 3\phi'$

Burton, Cabrera, and Frank [21] have further demonstrated that the number of atoms at a ledge, $n(L)$ is given by $n(L)_e$, even under conditions removed from equilibrium. Hence, even when $p < p_e$ (non equilibrium case), the mechanism is essentially the same since $r_1 >> r_5$. This conclusion was also established by Knacke and Stranski [9] for the geometry of a hard sphere model of a hexagonal surface, by estimating the transition probabilities for various atom movements.

2.4 (IV) Kinetics of Metal Evaporation

An expression for the evaporation rate can be derived if one solves the problem for the surface diffusion of atoms from ledge positions in a direction normal to the ledge (x direction). In applying equations (17) to (22) under non equilibrium conditions, Hirth and Pound[15] have shown that it is only necessary to write p for p_e and assume $n(L) = n(L)_e$ in equations (17), (20), (21), (22). However, in order to apply equations (18) and (19), it is necessary to obtain an expression for $n(s)$ which does not equal $n(s)_e$ due to surface diffusion away from a ledge. They were able to obtain such an expression by assuming $n(s) = n(s)_e$ near a ledge and solving the diffusion problem.

The solution of this problem by Hirth and Pound [15] is as follows. The net flux, J_v, into the vapour at any point on the surface is $r_3 - r_4$. Therefore,

$$J_v = n(s)\nu \exp(-\Delta F_3/kT) - p/(2\pi mkT)^{\frac{1}{2}} \qquad (23)$$

or at constant temperature,

$$J_v = C_1 n(s) - C_2 p \tag{24}$$

Since $n(s) = f(x)$, it is necessary to find a relation for $n(s)$ with respect to x. The net flux of atoms away from a ledge is,

$$J_s = - D_s \frac{dn(s)}{dx} \tag{25}$$

and since, $$- \frac{\partial J_s}{\partial x} = J_v, \tag{26}$$

$$\frac{d^2 n(s)}{dx^2} = (C_1/D_s) n(s) - (C_2/D_s) p \tag{27}$$

Incorporating the above assumption that $n(s) = n(s)_e$ near a ledge, and the fact that the distribution of adsorbed atoms under steady state conditions is symmetrical from ledge to ledge, a solution for $n(s)$ from equation (27) can be obtained with the following boundary conditions: $n(s) = n(s)_e$ at $x = 0$, $x = \lambda_o$ and $dn(s)/dx = 0$ at $x = \lambda_o/2$. Here, λ_o is the distance between two adjacent ledges.

It is now of interest to calculate $\langle n(s) \rangle_{average}$, since the result can be inserted into equation (24) to compute the net rate of evaporation. Hirth and Pound[15] give this result as:

$$\langle n(s) \rangle_{av} = (2/Q\lambda_o) \left[n(s)_e - C_3 p \right] \tanh(Q\lambda_o/2) \quad C_3 p \tag{28}$$

where Q and C_3 are constants.

The only unknown parameter is λ_o, preventing the determination of the net evaporation flux from:

$$J_v = C_1 \langle n(s) \rangle_{av} - C_2 p \tag{29}$$

λ_o may be estimated by considering the motion of

monatomic ledges on a crystal surface. It has been shown [15] that $\lambda_o \simeq 6/Q$, when the ledges have attained a steady state terminal velocity. This value can be substituted into equation (28) to obtain $\langle n(s) \rangle_{av}$.

It is more convenient to express the evaporation rate in terms of α which is given as :

$$\alpha = \frac{r_3 \ (p = p)}{r_3 \ (p = p_e)} = \frac{\langle n(s) \rangle_{av}}{n(s)_e} \qquad (30)$$

The result of this ratio has been shown [15] to be:

$$\alpha = 2/3 \ (p/p_e) + 1/3 \qquad (31)$$

Thus, it is seen that the condensation coefficient, at constant temperature, increases from 1/3 at p = 0, to unity at $p = p_e$. At p = 0, α is independent of temperature, and for finite values of p, α decreases with an increase in temperature due to an increase of the vapour pressure, p_e, with temperature. Nevertheless, the value never falls below 1/3. These conclusions only apply under the condition that the distance between sources of monatomic ledges at crystal edges or line imperfections is large relative to λ_o .

In their analysis, Hirth and Pound[15] have demonstrated that crystal edges do in fact serve as ready sources for ledges. These ledges attain a steady state maximum velocity on moving away from their sources, such that the terminal spacing is achieved at a distance X_o from the source, where $X_o \simeq 10 \ \lambda_o$. The authors emphasize that these conditions only apply for perfect metals, free of pores, cracks, screw dislocations,

macroscopic steps etc.

2.4 (V) The Effects of Various Physical Properties on the Condensation Coefficient

An increase in the evaporation rate, due to positive deviations from the rate limiting law (equation 31) should be expected for very small crystals, since the crystal edges serve as sources for ledges. According to the advanced theoretical considerations of the previous sections, a decrease in crystal size to the extent that its diameter is less than λ_o implies that the ledges can only attain a spacing of $\lambda < \lambda_o$. Consequently, an increased evaporation flux and a larger value for α may be expected as a result of equations (29) and (30). Nevertheless, this effect would only occur in crystals in the 1 to 100 micron range due to the small values of λ_o .[15] Pores and cracks may also serve as ledge sources and only act in decreasing the crystal size.

It is known, [21] that screw dislocations, emerging at crystal surfaces, play an important role in crystal growth, acting as sources of monatomic ledges. However, in crystal evaporation, edges etc. can act as ledge sources, and screw dislocations are not necessary. Hirth and Pound [30] have demonstrated that, at large undersaturations, except for a perturbed region near the point of intersection of a dislocation with the surface, the ledge spacing should approach λ_o as for ledges originating from crystal edges. Within the perturbed region (X_o), the terminal spacing of ledges (λ) is less than

λ_o , and positive deviations from the limiting rate law may occur in this area.

At small undersaturations, Hirth and Pound [30] demonstrated that the spacing between ledges is greater than λ_o , and hence, the limiting law holds for all concentrations of screw dislocations and temperatures.

It would be expected that an oxide film would altogether change the evaporation kinetics of metal crystals. It has been observed that the evaporation characteristics of Fe - Cr alloys [31] have not been upset by the presence of thin surface films. It is believed [15] that, at elevated temperatures, when the vapour pressures of metals are appreciable, adsorbed gas would be present in negligible amounts and would not seriously affect evaporation phenomena.

For an equilibrium crystal of the Gibbs - Wulff shape in equilibrium with its vapour at p_e, the evaporation rate per cm^2 per second is the same for each of the bounding crystallographic planes, which are in general, low index planes. When net evaporation is occurring ($p < p_e$), it can be shown that the evaporation rate is approximately the same for the low index planes. For high index planes, there are two possible effects; for small crystals, where surface free energy is a criterion in evaporation phenomena, the high index planes will be annihilated by atom movements through the vapour and by surface diffusion to low index planes, and hence, evaporation from the low index planes only need be considered. For large crystals,

it is thought that impurity adsorption at selective positions on high index planes, containing a large concentration of kinks, will poison active kink positions deactivating these planes with respect to low index planes, thus promoting the crystal to assume a shape bounded by low index planes. Again only the low index planes need be considered.

2.4 (VI) The Effects of Various Chemical Properties on the Condensation Coefficient

The presence of macroscopic ledges or striations on the surface of an evaporating crystal would be expected to alter the kinetics of that surface. Two schools of thought exist regarding the origin of these ledges, and, in both cases, the presence of an oxidizing agent is necessary.

Bènard and Moreau [32], after investigating the thermal etching characteristics of several Fe - Cr alloys, proposed, that if a metal surface is exposed to an atmosphere in which the partial pressure of the oxidizing agent (O_2 or H_2O) is less than the dissociation pressure of the oxide of the material, selective chemisorption will occur on the different crystal faces. As a result, the surface energy of various crystal faces is lowered. The appearance of striations may then occur, provided the temperature is sufficiently elevated to permit the reorganization of the surface by surface diffusion or some other process. According to the above authors, net evaporation is not necessary for the appearance of striations. The reduction in surface energy is the driving force for the reaction.

On iron, this reaction is reversible; the surface will striate if the atmosphere is slightly oxidizing, and becomes specular if the oxidizing agent is rigorously removed from the system. A critical gas composition defines a transition region at each temperature.

On the other hand, Hondros and Moore [33] have demonstrated that net evaporation in the presence of oxygen is a necessary factor to produce thermal etching on silver. They consider that the tendency to establish a minimum of surface energy is not the driving force of the process. In vacuum, pits are found on the surface, and in an inert gas the surface remains smooth.

These authors believe that the presence of macroscopic or polyatomic ledges is due to the coalescence of monatomic ledges. On evaporation, atoms are continually removed from the kink positions of the step edges and thus the monatomic ledges attain a drift velocity. It is felt that the impurity adsorption of oxygen retards the motion of ledges, allowing advancing ledges to group together to form a macroscopic ledge. Under conditions of evaporation and condensation, because the surface remains smooth, this poisoning effect, and hence, the grouping of ledges, does not occur.

It is of interest to point out the consequences of these views on the evaporation kinetics of metals. If polyatomic ledges act as a source for monatomic ledges, and, if their separation is only of the order of X_o, the distance of

the perturbed area, positive deviations from the rate limiting law would occur. We have previously shown in the description of evaporation kinetics that the condensation coefficient would then approach unity. Polyatomic ledges, however, formed as a result of oxygen poisoning, would not be expected to act as a source for monatomic ledges. In this case, the concentration of adsorbed atoms would decrease as grouping of the ledges occurred. Hence, the rate of evaporation would be lowered and one could expect negative deviations from the value of 1/3 for the condensation coefficient under the rate limiting conditions previously discussed.

2.5 Vapour Pressure Determinations of Iron and Chromium

2.5 (i) Introduction

In this section, the vapour pressure data reported in the literature for iron, chromium and the system iron-chromium are summarized. The chief methods used are the Knudsen cell and Langmuir free evaporation techniques, although the vapour pressure of chromium has been determined using a relatively unreliable boiling point method. In many cases, the data has been reported as ln p vs. 1/T plots. These curves will not be reproduced here; however, the results of such investigations will be compared to the more reliable data, where the vapour pressures have been reported as a function of temperature. In general the vapour pressure of a metal is expressed by an equation of the following type:

$$R \ln p = \left(\frac{F^{o}_{T} - H^{o}_{298}}{T}\right)_{cp} - \left(\frac{F^{o}_{T} - H^{o}_{298}}{T}\right)_{g} - \left(\frac{H^{o}_{v298}}{T}\right) \qquad (32)$$

where,

$$H_v^o(T) = H_v^o(298) + (H_T^o - H_{298}^o)_g - (H_T^o - H_{298}^o)_{cp} \qquad (33)$$

and from which, the heat of evaporation may be determined. The more reliable data on enthalpy changes are reported in the following sections.

2.5 (ii) Vapour Pressure Determinations of Iron

The vapour pressures of iron have been reported by Jones, Langmuir and MacKay[34], Marshall, Dornte and Norton[35], Edwards, Johnston and Ditmars[36], McCabe, Hudson and Paxton[8], and by Gulbransen and Andrew[31].

Jones et al. determined the vapour pressure of iron by the Langmuir method over the temperature range 1270°K to 1580°K, by measuring the rate of evaporation from filaments heated in a vacuum. The temperature of the filaments was measured with an optical pyrometer. Marshall et al. measured the free evaporation rate from inductively heated iron rings over the temperature range 1317°K to 1579°K at twelve temperatures. The results of these investigations were in agreement within the limits of experimental error, and the values for the heats of evaporation reported were 95,522 and 96,033 cal/gm. atom respectively.

Edwards et al., again employing the Langmuir method, measured the vapour pressure of iron from the rates of evaporation from inductively heated cylinders over the temperature range 1356°K to 1519°K. The values for the vapour pressures

obtained by these investigators are approximately one half the values obtained by Jones et al. and Marshall et al. The heat of evaporation at the absolute zero temperature was reported as 99,207 cal/mole. In this investigation, the authors expressed the vapour pressure as a function of temperature by the equation:

$$\log p = -\frac{21677}{T} + 0.0004438T - 0.0000003157T^2 + 7.5918 \qquad (34)$$

McCabe et al. determined the vapour pressure of iron by the Knudsen cell method over the temperature range 1495°K to 1510°K. The results of this investigation were in good agreement with those of Edwards et al. The results obtained by Edwards et al. and McCabe et al. demonstrate that the Knudsen cell and Langmuir free evaporation methods agree at elevated temperatures within the limits of experimental error. They concluded that the condensation coefficient for iron must be between 0.8 and 1.0.

Rencently, Gulbransen and Andrew determined the vapour pressures of iron by the Langmuir method over the temperature range 1025°C to 1150°C. The evaporation rates were measured, utilizing a sensitive microbalance, in a vacuum of 10^{-8} mm. Hg. The vapour pressures calculated in this investigation were lower than those reported by Edwards et al. and McCabe et al. The heat of evaporation at absolute zero was reported as 100.5 kcal/mole.

Elliott and Gleiser,[37] in their text "Thermochemistry for Steelmaking", have reported the most probable values of

the constants in equation (32). The heat of evaporation at 298°K for iron, compiled from the data of Morris et al.[38], is 99,610 ± 200 cal/gm. mole. We have employed these results for the determination of the vapour pressure of iron in the temperature range of this investigation.

2.5 (iii) Vapour Pressure Determinations of Chromium

The vapour pressures of chromium have been determined by Bauer and Brunner[39], Speiser, Johnston and Blackburn[40], McCabe, Hudson and Paxton[8], Kubaschewski and Heymer[41], and Gulbransen and Andrew[31].

Bauer et al. reported the first experimental determinations of the vapour pressures of pure chromium. The vapour pressures were determined by a boiling point method and are not considered to be reliable as compared to the results of more recent investigations.

Speiser et al. determined the vapour pressures of chromium over the temperature range 1283°K to 1561°K. In this case the Langmuir technique was employed and the rates of evaporation were computed from the weight loss of inductively heated annular rings. The heat of evaporation at absolute zero was reported as 93.5 kcal/mole and the vapour pressure was expressed as a function of temperature:

$$\log p \text{ (atm)} = - \left(\frac{20,473}{T}\right) + 7.467 \qquad (35)$$

McCabe et al. determined the vapour pressure of chromium over the temperature range 1435°K to 1505°K using

the Knudsen cell method. The results of this investigation were in good agreement with those of Speiser et al. This fact demonstrates, as in the case for iron, that the condensation coefficient for chromium should be between 0.8 and 1.0.

Kubaschewski et al. determined the vapour pressures of chromium over the temperature range 1170°C to 1397°C. In this case, the investigators used a Knudsen cell in conjunction with a radioactive tracer technique, in order to obtain the rates of effusion of chromium through the cell orifice. Excellent agreement was obtained with the results of Speiser et al. and McCabe et al. The vapour pressure of chromium was expressed within a reliability of $\pm$ 20percent as:

$$\log p \text{ (atm)} = - \frac{19700}{T} + 6.92 \qquad (36)$$

Recently, Gulbransen et al. obtained the vapour pressures of chromium over the temperature range 1000°C to 1100°C, employing a vacuum microbalance for the determination of the rates of free evaporation. The results of this investigation, carried out in a vacuum of 10^{-8} mm. Hg, were slightly lower than earlier reported data. The heat of evaporation for chromium at absolute zero was given as 95.4 kcal/mole.

In this investigation, we have employed the constants given by Eliott and Gleiser[37] for equation (32) to calculate the vapour pressures of chromium in the temperature range 900°C to 1100°C. The heat of evaporation for chromium at 298°K is 94,850 $\pm$ 500 cal/gm. mole.

2.6 The Vapour Pressure Determinations of the System Iron - Chromium

2.6 (i) Introduction

The results of vapour pressure determinations of alloys are not only of importance per se but allow the calculation of chemical activities and other pertinent thermochemical data. The Knudsen and Langmuir methods are particularily suitable for the determination of vapour pressures of alloys at elevated temperature, whenever the vapour can be collected and analyzed for the evaporating species. In this section, the results of previous investigations on the system iron - chromium are presented along with other pertinent data.

2.6 (ii) The Vapour Pressures of Iron - Chromium Alloys

The vapour pressures of iron - chromium alloys have been determined by McCabe et al.[8], Kubaschewski et al.[41], and more recently, by Gulbransen et al.[31]

McCabe et al. determined the total vapour pressures of several iron - chromium alloys over the temperature range 1207°C to 1249°C, utilizing the Knudsen technique. Since all attempts to collect and analyse the vapour for chromium failed, the Knudsen equation had to be slightly modified. The equation can be written as:

$$P_T = P_{Cr} + P_{Fe} = \frac{\sqrt{2\pi RT}}{At}\left(\frac{W_{Cr}}{\sqrt{M_{Cr}}} + \frac{W_{Fe}}{\sqrt{M_{Fe}}}\right) \qquad (37)$$

Since the weight losses of chromium and iron were not determined separately the Knudsen equation was written as:

$$p_T = \sqrt{\frac{2\pi RT}{M_{av}}} \cdot W_T \qquad (38)$$

where $$W_T = W_{Cr} + W_{Fe} \qquad (39)$$

$$\sqrt{M_{av}} = \left[\frac{(M_{Fe} + M_{Cr})}{2}\right]^{\frac{1}{2}} \qquad (40)$$

Total pressures were determined for alloys ranging in chromium content from 17.9 percent to 77.1 percent at 1207°C and one determination was made at 1249°C.

The activities of chromium were estimated on the basis of regular solution theory. According to this theory, the activity coefficient of chromium in iron - chromium alloys can be expressed as:

$$\gamma_{Cr} = e^{\beta N_{Fe}^2} \qquad (41)$$

Likewise, the activity coefficient for iron can be written as:

$$\gamma_{Fe} = e^{\beta N_{Cr}^2} \qquad (42)$$

where γ is the activity coefficient, N is the mole fraction, and β is a constant.

The value of β, and hence, the activities were estimated from the experimental data, after appropriate substitutions had been made in the Knudsen expression, namely:

$$W_T = (p^o_{Cr} N_{Cr}\, e^{\beta N_{Fe}^2} \sqrt{M_{Cr}} + p^o_{Fe} N_{Fe}\, e^{\beta N_{Cr}^2} \sqrt{M_{Fe}}) \frac{At}{(2\pi RT)^{\frac{1}{2}}} \qquad (43)$$

where p^o is the vapour pressure of the pure component, A is the orifice area, and t is the exposure time.

The activities calculated by this method are given in Table II (a). In the temperature range 1200°C to 1250°C, the

ACTIVITIES IN THE IRON - CHROMIUM SYSTEM

TABLE II (a)

Temperature (°C)	N_{Cr}	A_{Cr}
1370	0.0513	0.115
1355	0.0474	0.112
1341	0.0436	0.107
1370	0.0398	0.100
1355	0.0828	0.153
1341	0.0813	0.151
1370	0.0798	0.146
1341	0.2973	0.398
1370	0.2965	0.391
1355	0.2955	0.402
1355	0.2945	0.402
1370	0.501	0.528
1355	0.501	0.543
1341	0.5005	0.534
1370	0.699	0.712
1355	0.699	0.727
1370	0.2983	0.391

TABLE II (b)

Temperature (°C)	N_{Cr}	A_{Cr}
1205	0.756	0.764
1206	0.271	0.304
1208	0.177	0.216
1205	0.178	0.242
1206	0.558	0.569
1211	0.409	0.393
1207	0.133	0.164
1249	0.165	0.168

iron - chromium system shows only small positive deviations from Raoult's Law, that is, the thermodynamic behaviour of iron and chromium in the system iron - chromium is close to ideal over the temperature range investigated.

Kubaschewski et al. directly determined the partial pressures of chromium over several iron - chromium alloys at 1341°C, 1355°C and 1370°C, utilizing the Knudsen technique and a radioactive tracer method to analyse for the chromium contents of the vapour. The activities of chromium were calculated, and again, only small positive deviations from Raoult's Law occurred. These results are given in Table II (b). Although the activities determined by Kubaschewski et al. are slightly higher than the values reported by McCabe et al., the results of the two investigations are in good agreement. In view of the fact that Kubaschewski et al., determined the partial vapour pressures of chromium directly, their results are considered to be more reliable than those of McCabe et al.

Gulbransen and Andrew recently determined the vapour pressures of an iron - 21.9 percent chromium alloy over the temperature range 920°C to 1040°C, utilizing the Langmuir free evaporation method. The weight losses were determined using a vacuum microbalance technique, the residual pressure in the experimental apparatus being 10^{-8} mm. Hg. In contrast to McCabe et al. and Kubaschewski et al., Gulbransen's values for the total vapour pressure are less than the values calculated on the basis of ideal behaviour. Although the values reported are close to ideal, these results show that the apparent

negative deviations from Raoult's Law are associated with the erroneous assumption that the condensation coefficient is equal to unity over the temperature range investigated.

CHAPTER III

EXPERIMENTAL APPARATUS AND PROCEDURE

3.1 Experimental Apparatus

Three types of apparatus were employed in this investigation. For the initial stages of the experiments a vacuum assembly was constructed for measurements of free evaporation rates. This assembly was then equipped with a Knudsen cell for vapour effusion measurements. Finally, a hot stage microscope assembly was constructed for observations at temperature of the alloy surface during the process of evaporation.

A general view of the apparatus used for all vapour pressure determinations is shown schematically in Figure 2. The furnace section was of relatively simple construction. Power was supplied from a 2,500 VA transformer to the 20 inch Kanthal resistance heating element. This element was packed in a cylindrical ceramic protection tube with an aluminum silicate powder. A six inch layer of heat insulating brick was fitted around the protection tube. The remainder of the space between the layer of heat insulating brick and the outer transite walls was filled with mica for additional insulation. This heating assembly proved to be quite satisfactory throughout the course of experimental tests.

A Philips controlling instrument was utilized to control the temperature for an experiment to a pre-assigned constant

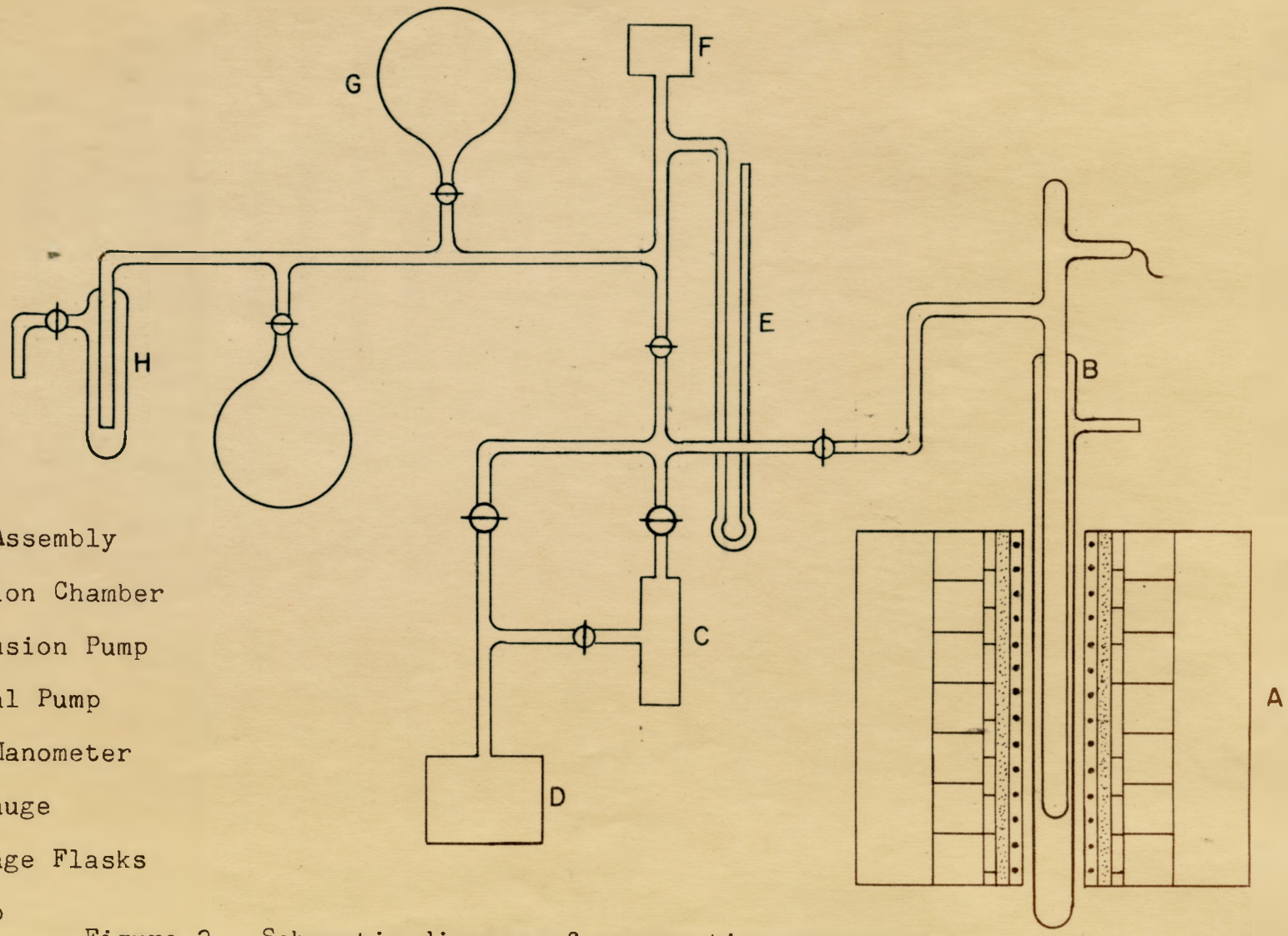

A - Furnace Assembly

B - Evaporation Chamber

C - Oil Diffusion Pump

D - Mechanical Pump

E - Mercury Manometer

F - McLeod Gauge

G - Gas Storage Flasks

H - Cold Trap

Figure 2. Schematic diagram of evaporation apparatus

value in the heating chamber. Any temperature fluctuation was sensed by a chromel-alumel thermocouple positioned in the hot zone. The voltage increment was relayed to the controlling instrument which, in turn, activated or deactivated a mercury plunger relay in the power circuit. The temperature in the reaction chamber was controlled to $\pm$ 1°C by this system.

The reaction hot zone, for the suspension of specimens to be evaporated, measured 2 inches with no variations in temperature to the experimental precision of $\pm$ 1°C, and 4 inches with only $\pm$ 2°C variation over this length. The central position of the hot zone varied from 10 inches at 700°C to 11 inches at 1100°C, as measured from the furnace top. This arrangement was suitable for all tests.

An enlarged view of the reaction tube section is shown in Figure 3. Originally, only a vacuum tight mullite tube was employed as a reaction chamber. However, it was discovered that the evaporating material attacked the tube walls giving rise to wall porosity and leakage from the atmosphere. The system was then modified, and this form is that shown in Figure 3. The outer mullite tube was sealed directly to the pyrex vacuum train. A fused quartz tube was inserted into the mullite tube and sealed to the pyrex walls utilizing a graded seal. The vacuum train was so arranged that a vacuum was produced in both the inner and outer regions of the quartz tube. This was done in order to prevent its collapse at high temperatures. As shown in Figure 3, the upper portion of the reaction

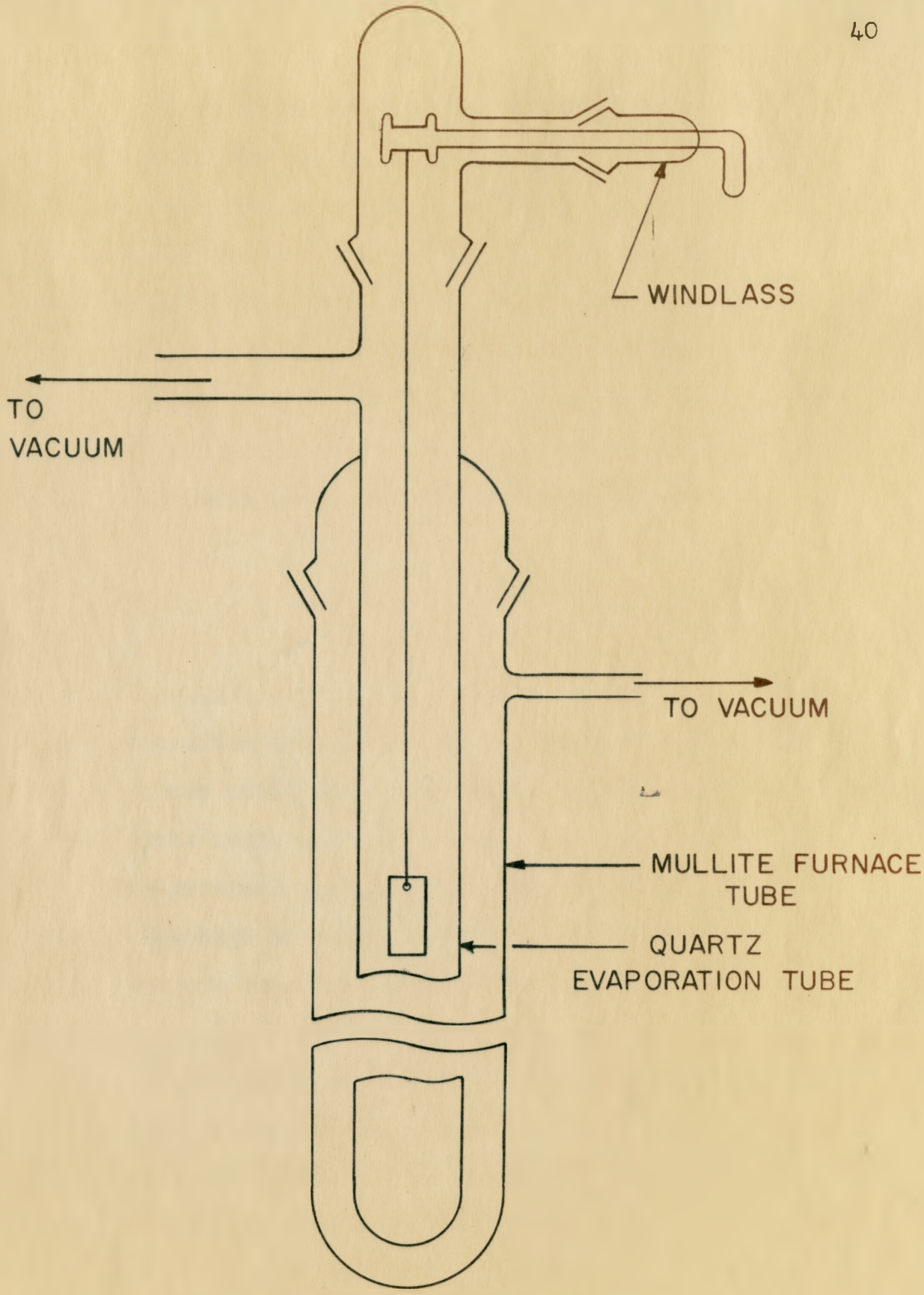

Figure 3. Evaporation tube

tube consists of a ground glass joint fitted with a male union containing a windlass. This permitted the rapid raising and lowering of the specimens without breaking the vacuum. For example, a sample could be raised from or lowered into the reaction zone within 30 seconds.

The pyrex vacuum train is clearly illustrated in Figure 2. It serves to connect the other components of the system with the pumping equipment, and contains the necessary valves, cold traps and gas storage flasks for experimental operations.

The vacuum pumping section consists of a water cooled, two stage oil diffusion pump backed by a single stage rotary pump. With this combination, a vacuum of 10^{-6} mm. Hg could be obtained after the necessary outgassing period. Another rotary pump was utilized to evacuate the previously mentioned quartz-mullite region.

The pressure measuring section consisted of a mercury manometer for high pressure measurement, and a McLeod gauge for low pressure measurement. The McLeod gauge was capable of measuring a vacuum of 10^{-6} mm. Hg.

For the vapour pressure determinations by the rate of effusion method, Knudsen cells were fabricated from molybdenum and "pyrophyllite" (a refractory aluminum silicate). This latter cell was constructed to determine whether there was an influence of the material on the effusion measurements. The construction was the same for both types of cells and,

consequently, only the fabrication of the molybdenum cell is given.

A schematic illustration of the cell is shown in Figure 4. The cell body was machined from a 3/8 inch diameter rod, threaded on the outside surface to accept a retaining cap, and was bored with a 5/16 inch diameter drill. The retaining cap was machined to size from a 1/2 inch molybdenum rod and threaded on the inside surface to fit the cell body. A small rim was retained on the cap and was drilled to accept two quartz suspension hooks. An orifice was formed in a 3/8 inch diameter, 3 mil molybdenum sheet by deforming the disc at its mid-point with a sharp punch. This operation formed a small nipple, the tip of which was then filed away until a small knife - edged hole appeared. The hole diameter was then measured on a projection microscope. The disc fitted the rim of the cell body, and when the retaining cap was screwed in place, a gas tight seal was formed. The complete cell was then suspended from the windlass into the hot zone by platinum wire.

Several tests were performed utilizing a hot stage assembly which fitted atop a Riechert projection microscope. A schematic illustration of the hot stage assembly is shown in Figure 5. The stage body was constructed from wrought brass containing a vycor window, fitted to the stage base by means of an "O"ring and a retaining cap. The "lid" contained teflon insulators through which the water cooled copper electrodes were inserted. The lid was attached to a flange on the stage

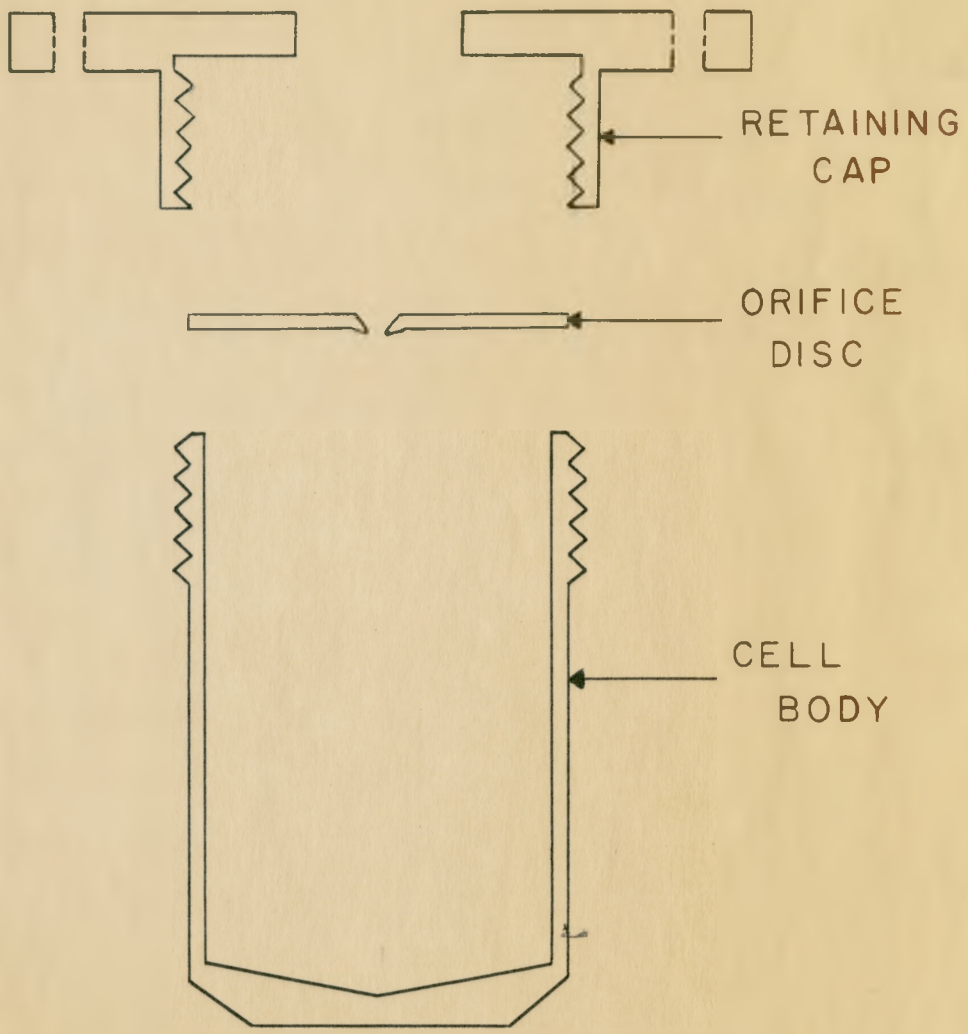

Figure 4. Schematic diagram of Knudsen cell

A - Cu Electrodes
B - Sample Holder
C - Sample
D - Thermocouple
E - Mo Heater
F - Mo Radiation Shield
G - Anti - Fog Shield
H - Vycor Window
I - Objective

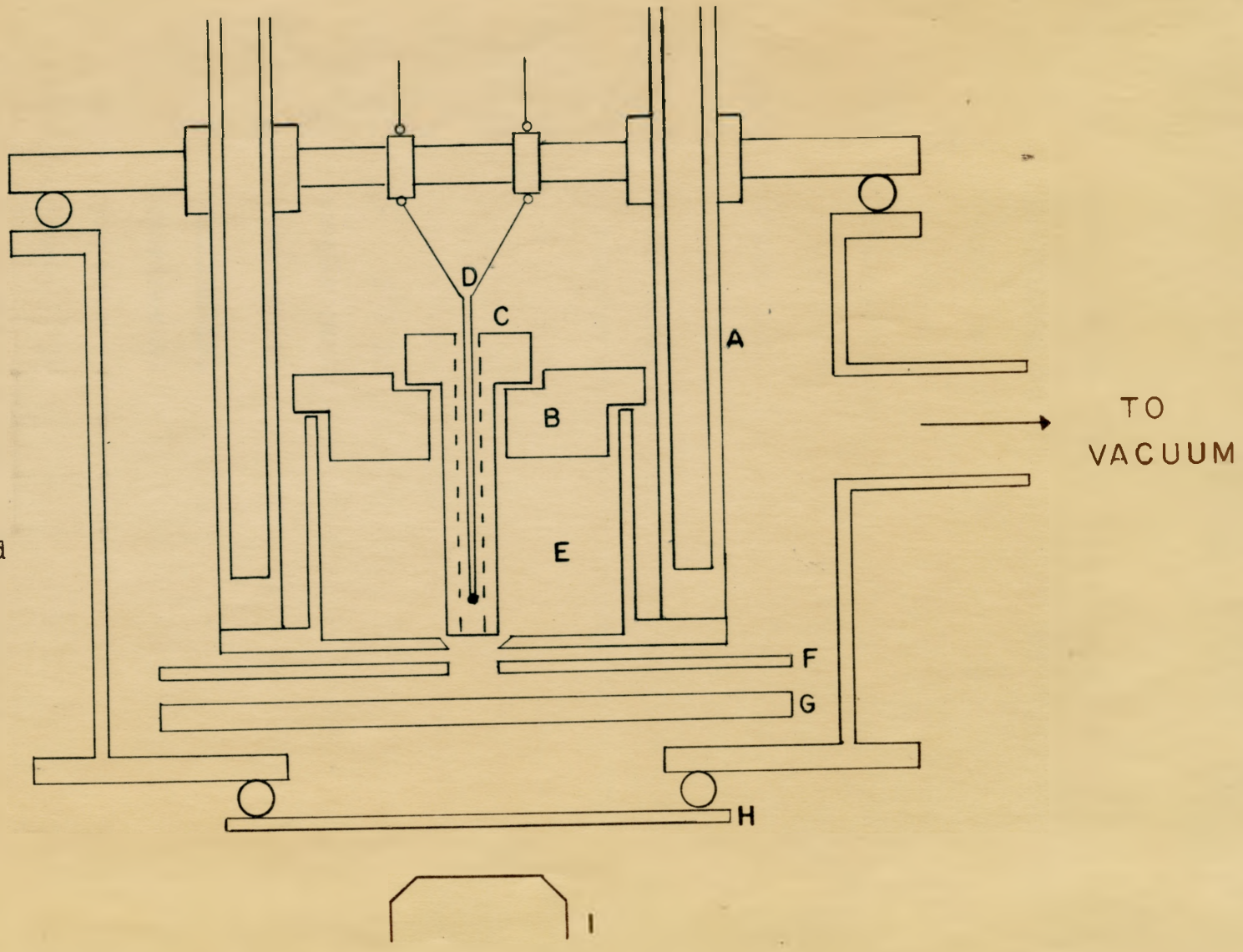

Figure 5. Schematic diagram of hot stage assembly

casing by means of an "O" ring and retaining bolts. A rectangular molybdenum heating element was connected to the electrodes by copper bus bars. A pryophyllite sample holder was machined to fit on the edges of the heating element, and to accept a machined sample, as demonstrated in Figure 5.

The vycor window was protected from heat and vapour by a molybdenum radiation shield and a movable quartz optical flat. The unit, in position on the microscope stage, was evacuated by an oil diffusion pump in conjunction with a rotary pump. The heating power was supplied from a transformer controlled by a powerstatt. The temperature was measured with a platinum - platinum, 10 percent rhodium thermocouple positioned in a hole bored into the specimen. The temperature was controlled to $\pm$ 5°C in this manner. The metallographically polished sample surface could then be viewed, at temperature, employing the optical system of the projection microscope.

3.2 Experimental Procedure

Experimental tests were carried out on the iron - 5 percent and iron - 25 percent chromium alloys in the apparatus described above. In the Langmuir tests, the samples used were cut from 5 mil thick alloy sheet supplied in the cold worked condition. The surface preparation consisted of abrasion with four grades of silicon carbide polishing paper ranging from 0/0 to 4/0. The sample dimensions were determined with a micrometer for computation of surface area (area range was approximately 3.5 cm^2). After thorough degreasing in acetone

for at least one hour, the samples were dried in an air blast and weighed on a microbalance to a precision of $\pm$ 2 μg.

Immediately after weighing, the specimens were attached to a platinum suspension wire, placed on the windlass of the reaction cell assembly and lowered into the hot zone, after a vacuum of at least 5 x 10^{-6} mm. Hg had been attained. All tests of the Langmuir free evaporation type were preceded by a two hour vacuum anneal at 800°C. Time zero was recorded after the test temperature was attained. A serious error was not introduced in the measurements of weight loss during the heating period from 800°C to the test temperature, since the furnace was capable of attaining the minimum temperature of 900°C and the maximum of 1080°C in 5 minutes and 20 minutes, respectively. After the prescribed time period, the samples were removed from the hot zone, cooled in a vacuum, weighed and examined microscopically under normal and oblique illumination. All surface features were then recorded and weight losses calculated.

Knudsen tests were carried out on the iron-25 percent chromium alloy. Sample preparation consisted of collecting alloy chips produced by a machining operation followed by thorough degreasing in acetone. The cell, illustrated in Figure 4, after outgassing at 1150°C for 50 hours and at 1550°C for 15 minutes, was filled to the 3/4 level with the sample chips, weighed and suspended by platinum wire and quartz suspension hooks on the windlass in the reaction tube. The same

evaporation procedure as used above was employed with the exception of the omission of the two hour annealing period. After the test period, the cell and charge was weighed and the weight loss computed.

Hot stage experiments were performed on the iron - 25 percent chromium alloy in order to follow morphological changes at the test temperature. A cylindrical sample was machined from alloy stock to the dimensions required by the holder and heating element geometry. It was then abraded with silicon carbide paper with water as lubricant followed by a polishing operation employing a 0.1 μ alumina slurry on a selvyt cloth. The specimen was then placed in position as shown in Figure 5. A thermocouple was placed into a hole bored in the specimen, so that its temperature could be recorded. Upon evacuation of the system, the power was turned on to the heating element and the test temperature attained in approximately 5 minutes. The temperature was checked and corrected, if necessary, every 15 minutes. Changes in surface morphology were followed visually, and photographed at various time intervals.

A complete chemical analysis of the alloys used in this investigation is given in the Appendix.

CHAPTER IV

EXPERIMENTAL RESULTS

4.1 Introduction

In this section, the results of our investigations on the evaporation kinetics of the iron - 5 percent chromium alloy and the iron - 25 percent chromium alloy are summarized graphically. The reported data apply to the temperature range 900°C to 1080°C; experimental tests were conducted at 900°C, 950°C, 1000°C, 1035°C and 1080°C for both alloys. Since a phase transformation occurs on the iron - 5 percent chromium alloy at 855°C[42], the structure being body centred cubic below 855°C, and face centred cubic above this temperature, the alloy was in the austenitic state for the experimental tests. The iron - 25 percent chromium alloy undergoes no transformations at temperatures below the melting point and, therefore, was in the ferritic state throughout the course of experiments. The prominent surface features of specimens subjected to free evaporation are reported and illustrated by photomicrographs taken under normal and oblique illumination. The features are further amplified by interference photographs of appropriate areas, and a photographic sequence of an iron - 25 percent chromium specimen under evaporation conditions employing hot stage microscopy techniques (see Figure 5).

4.2 Evaporation of an Iron - 5 Percent Chromium Alloy in the Temperature Range 900°C to 1080°C

4.2 (i) Evaporation Kinetics

The free evaporation kinetics of the iron - 5 percent Cr alloy are summarized graphically in Figure 6, and tabulated measurements are given in Table III. Each open circle on the graph represents a separate determination. The results show that the weight loss of the alloy (mg/cm^2) was directly proportional to time, and that linear kinetics obtain for tests up to 90 hours at 900°C and 10 hours at 1080°C. As to be expected, the rate of evaporation increased with increasing temperature.

4.2 (ii) Surface Topography

After all tests, the surface topography of each specimen was examined microscopically. Under normal illumination only coarse features were observed such as grain boundary delineation, abrasion scratches, a result of the method of preparation, and twinned regions. These observations are illustrated by Figures 7 (a) and 7 (b), which are photomicrographs of iron - 5 percent chromium alloy specimens evaporated for 2 hours and 15 hours respectively at 1000°C. In both cases, the magnification is 120 times. In Figure 7 (a), grain boundary delineation and preparation scratches are readily observed. In Figure 7 (b), however, grain boundary grooving is more prominent and the preparation scratches are not as evident as in Figure 7 (a). Also, twinned regions are illustrated by Figure 7(b).

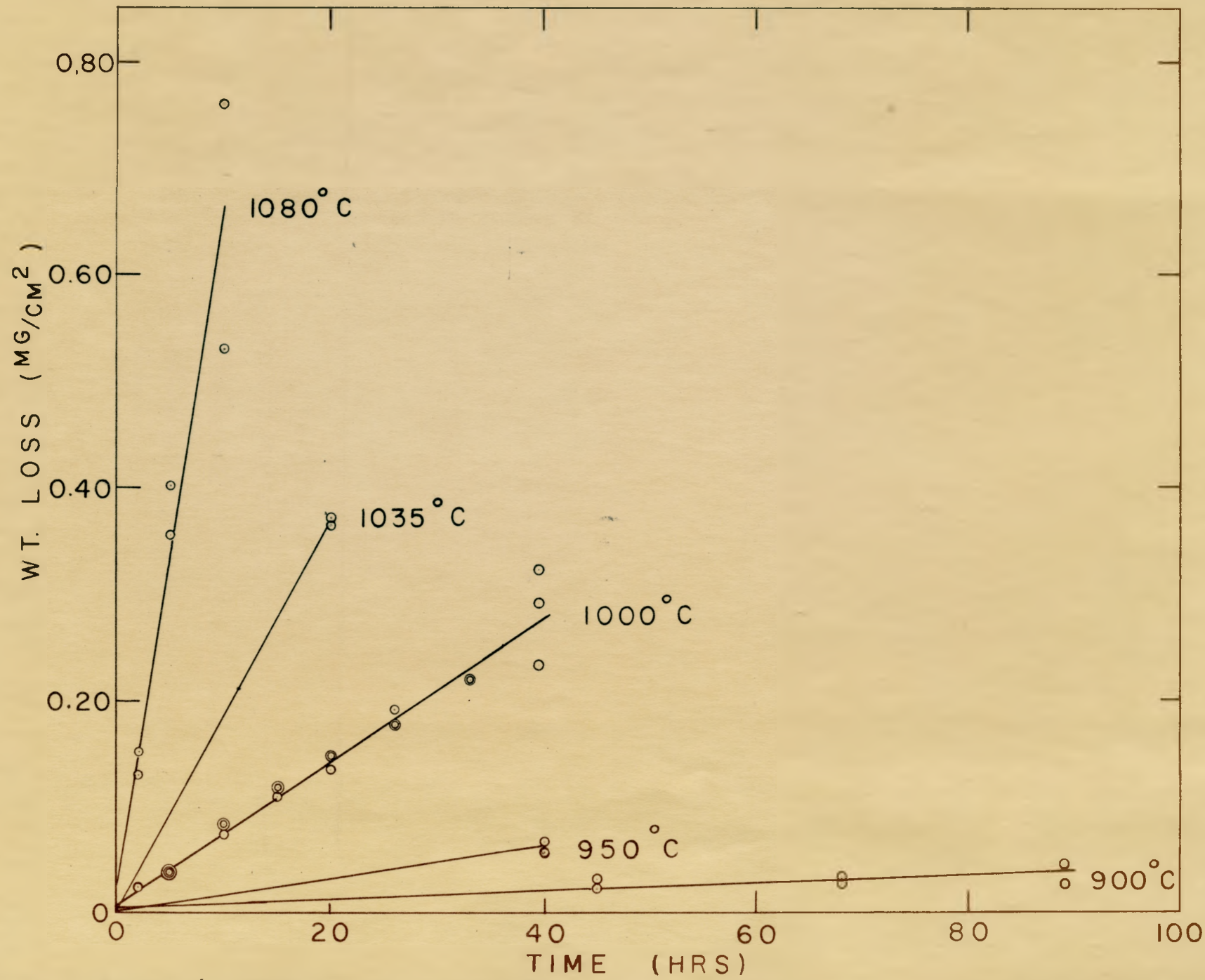

Figure 6. Free evaporation kinetics for the iron - 5 percent chromium alloy

TABLE III

WEIGHT LOSS MEASUREMENTS / IRON - 5 PERCENT CHROMIUM ALLOY

Run Number	Temperature (°C)	Time (Hrs)	Weight Loss (mg/cm^2)
1a	900	45	0.023
1b	900	45	0.032
2a	900	68	0.031
2b	900	68	0.028
3a	900	89	0.027
3b	900	89	0.048
4a	950	40	0.066
4b	950	40	0.057
5a	1000	2	0.019
5b	1000	2	0.022
6a	1000	5	0.037
6b	1000	5	0.038
6c	1000	5	0.039
7a	1000	10	0.081
7b	1000	10	0.073
7c	1000	10	0.082
8a	1000	15	0.118
8b	1000	15	0.110
8c	1000	15	0.118
9a	1000	20	0.134
9b	1000	20	0.143
9c	1000	20	0.147

TABLE III

(Cont'd)

WEIGHT LOSS MEASUREMENTS / IRON - 5 PERCENT CHROMIUM ALLOY

Run Number	Temperature (°C)	Time (hrs)	Weight Loss (mg/cm^2)
10a	1000	26	0.190
10b	1000	26	0.172
10c	1000	26	0.175
11a	1000	33	0.219
11b	1000	33	0.218
12a	1000	39.5	0.290
12b	1000	39.5	0.232
12c	1000	39.5	0.322
13a	1035	20	0.365
13b	1035	20	0.321
14a	1080	2	0.152
14b	1080	2	0.130
15a	1080	5	0.356
15b	1080	5	0.400
16a	1080	10	0.760
16b	1080	10	0.530

(a) Evaporated for 2 hours

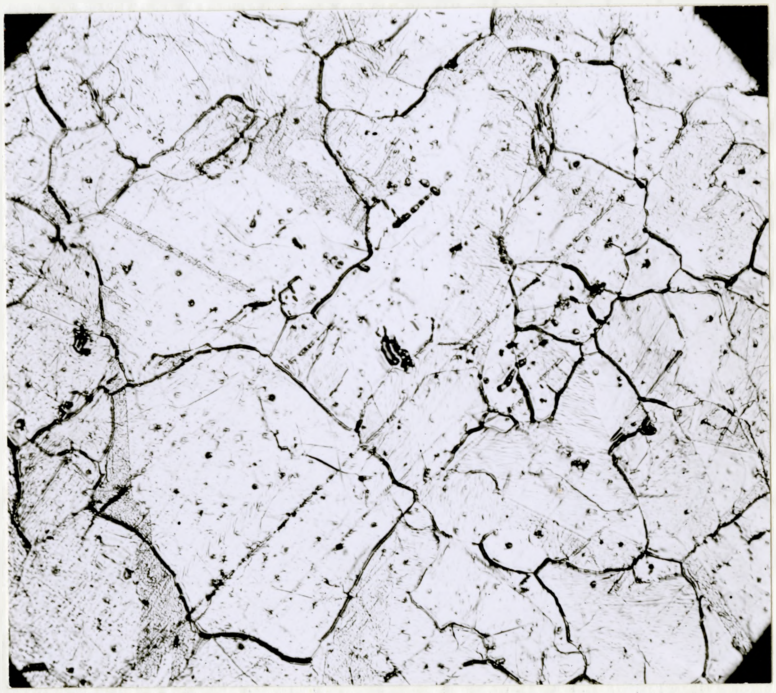

(b) Evaporated for 15 hours

Figure 7. Surface topographies of Fe-5 percent Cr specimens evaporated at 1000°C; X 120.

The fine surface detail was not observable under normal illumination and, therefore, the specimens were viewed under oblique illumination. The results of these observations are summarized in the following photomicrographs. Figure 8 illustrates the general appearance of the surface of a specimen evaporated at low weight losses, for 68 hours at 900°C. The magnification is 1080 times. This photomicrograph demonstrates the observed types of features, namely, regions of coarse surface faceting, regions of wavy contours, regions of parallel contours and specular regions. Grain and twin boundary delineation is also illustrated. The twinned region, crossing the coarse faceted grain, clearly demonstrates the effect of orientation on surface structure. This striated surface is characteristic of specimens of the iron - 5 percent chromium alloy, evaporated at temperatures from 900°C to 1035°C for the exposure times given by Figure 6. Specular regions were present on all surfaces but are in the minority over this temperature range. At the highest investigated temperature of 1080°C for long exposure times, specular regions were more abundant, and the striated regions did not show the prominent contours observable at lower temperatures. A photomicrograph (1080 X) of a typical surface area of a specimen evaporated for 10 hours at 1080°C is shown in Figure 9. It is obvious that the striated regions are in the minority and that the contour formations are not as distinct as those demonstrated in Figure 8.

The alteration of surface appearance with temperature

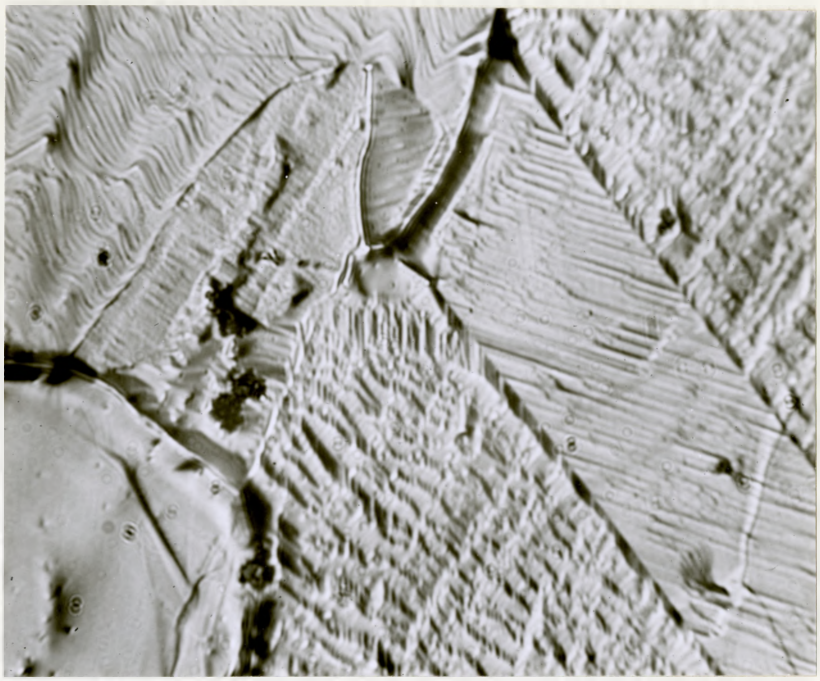

Figure 8. Surface topography of an Fe-5 percent Cr specimen evaporated at 900°C for 68 hours; X 1080 (oblique)

Figure 9. Surface topography of an Fe-5 percent Cr specimen evaporated at 1080°C for 10 hours; X 1080 (oblique)

from a striated morphology to a specular morphology is further demonstrated in Figures 10 (a), 10 (b), 10 (c), 10 (d), and 10 (e), representing appropriate areas of specimens evaporated at 900°C for 68 hours, 950°C for 40 hours, 1000°C for 26 hours, 1035°C for 20 hours and 1080°C for 10 hours respectively. The magnification in all cases is 760 times. This sequence not only demonstrates the surface transformation effect with temperature, but also supplies physical evidence for the striated appearance of surfaces of specimens evaporated in the austenitic state for the temperature range investigated.

It was also observed that the striations on the 5 percent alloy could be eliminated by a prolonged anneal in the ferritic range. This effect is demonstrated in Figure 10 (f) (1080 X), which illustrates the surface of a specimen originally evaporated for 68 hours at 900°C (10 a) then evaporated at 840°C for 70 hours. It is evident that the surface has undergone transformation from a striated to a specular appearance. At the maximum investigated temperature, this transformation appeared to be time dependent. This observation is demonstrated by the photomicrographs at a magnification of 1080 X in Figure 11 (a) and 11 (b), representing surfaces of specimens evaporated for 2 hours and 5 hours respectively, at 1080°C. These observations and those represented in Figure 10 (e) illustrate the time dependence, at constant temperature, of the surface appearance. Thus, the results indicate that the transformation from a striated to a specular surface occurs

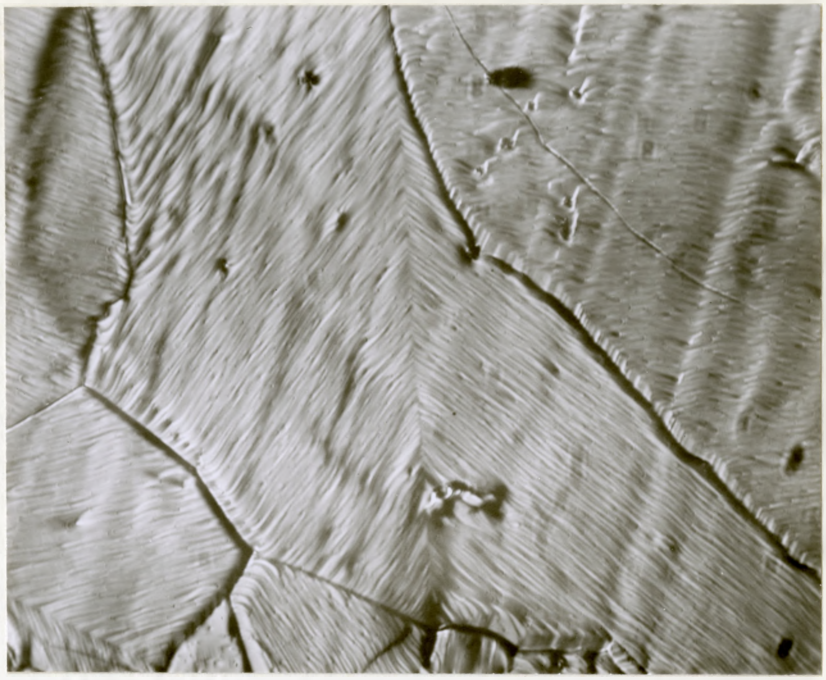

(a) Evaporated at 900°C for 68 hours

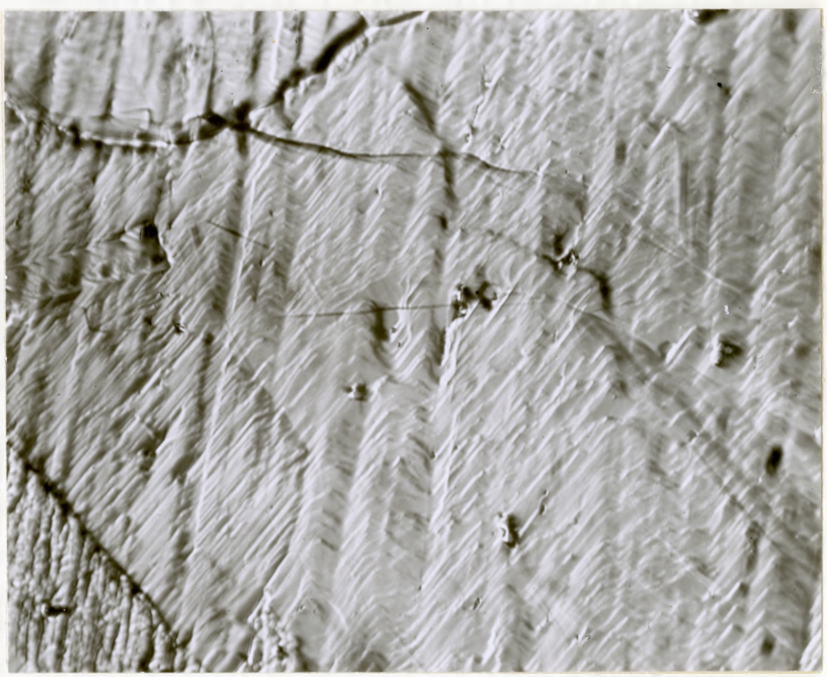

(b) Evaporated at 950°C for 40 hours

Figure 10. Surface topographies of Fe-5 percent Cr specimens; X 760 (oblique)

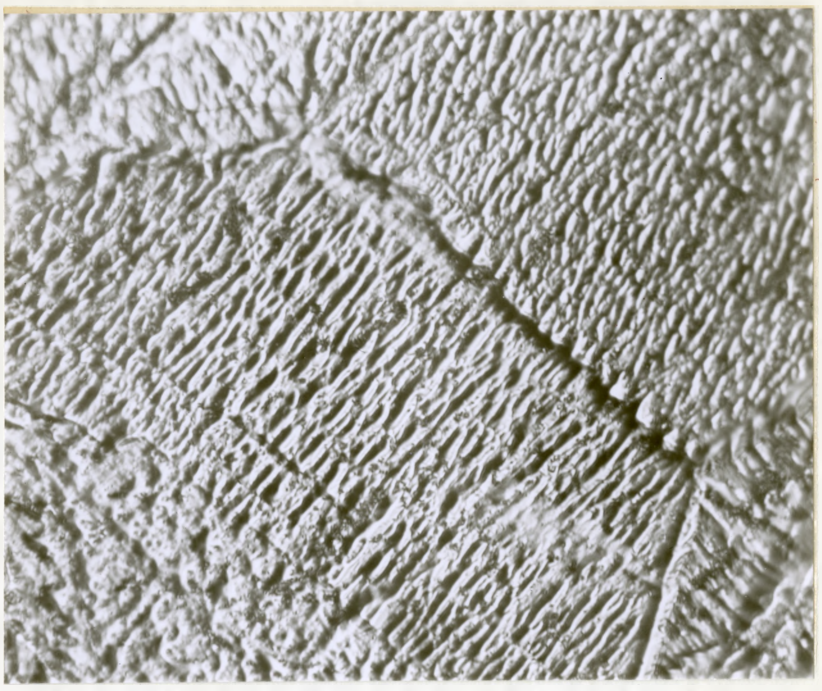

(c) Evaporated at 1000°C for 26 hours

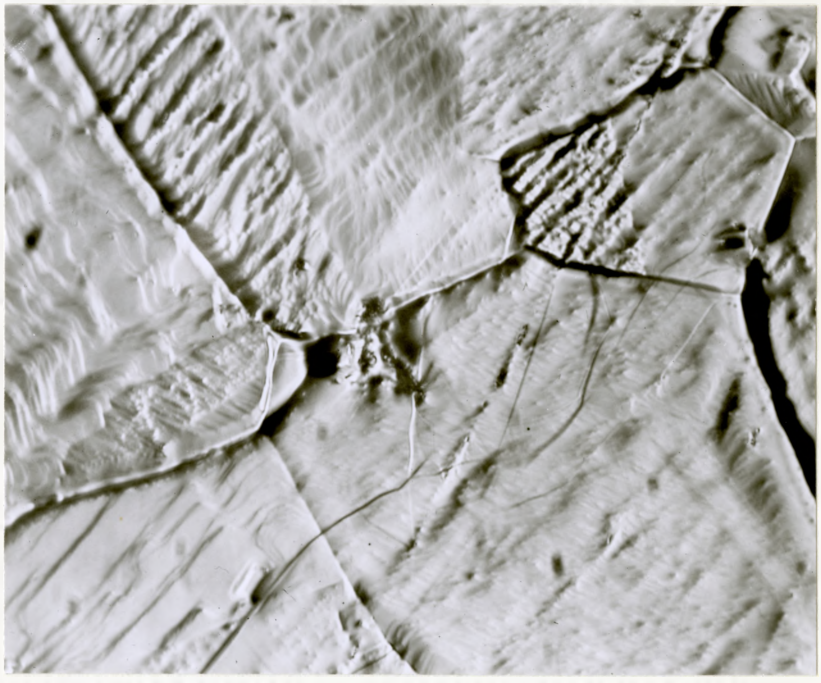

(d) Evaporated at 1035°C for 20 hours

Figure 10. Surface topographies of Fe-5 percent Cr specimens; X 760 (oblique)

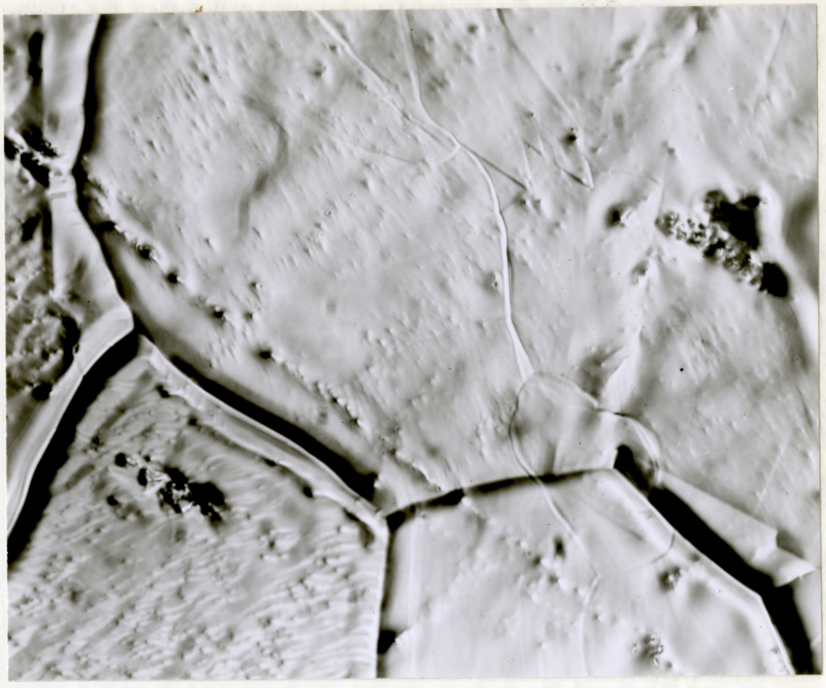

Figure 10 (e) Evaporated at 1080°C for 10 hours

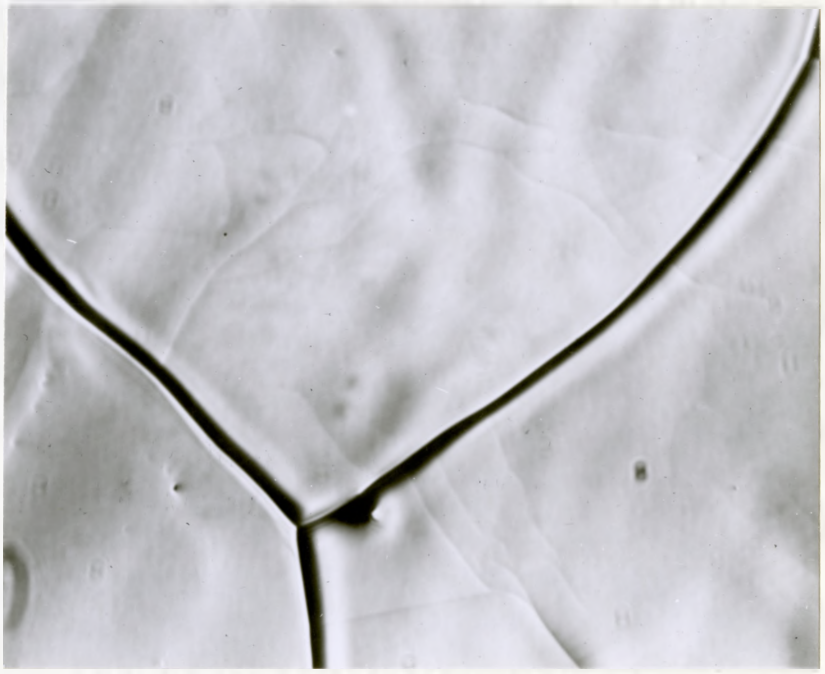

Figure 10 (f) Evaporated at 900°C for 68 hours and at 840°C for 70 hours; X 1080 (oblique)

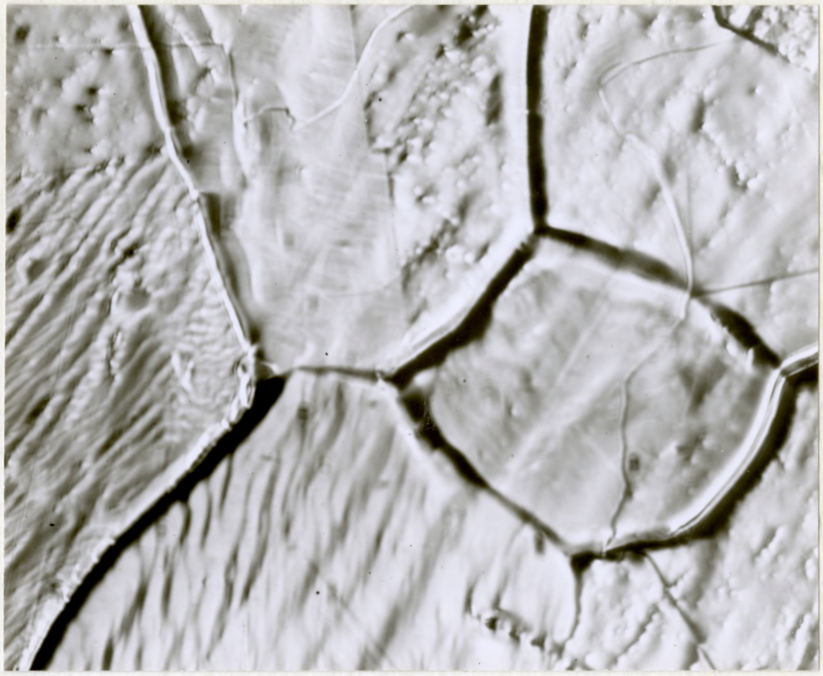

(a) Evaporated at 1080°C for 2 hours

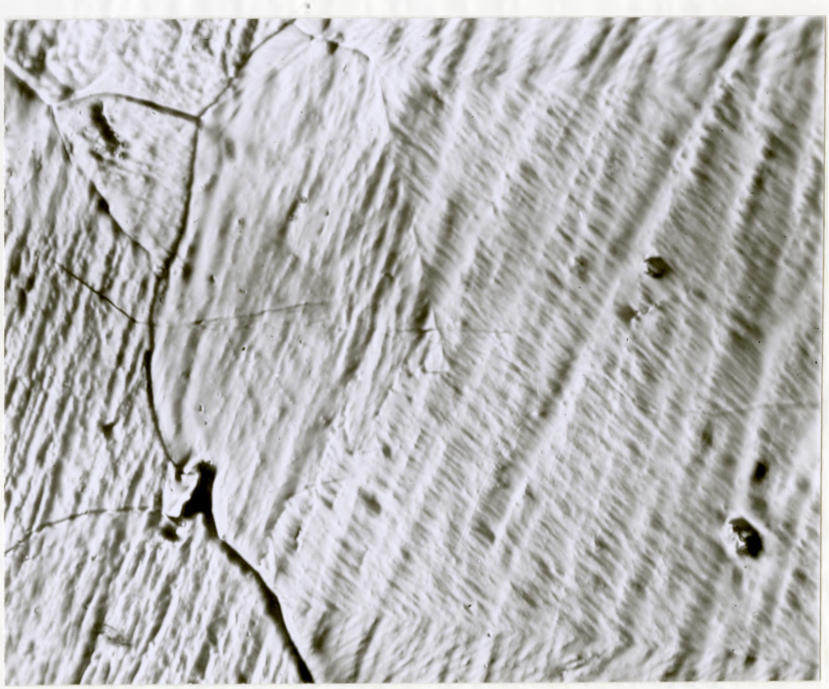

(b) Evaporated at 1080°C for 5 hours

Figure 11. Surface topographies of evaporated Fe-5 percent Cr Specimens; X 1760 (oblique)

with increasing temperature, and that this transformation also occurs at the maximum temperature investigated, with increasing time.

Finally, the evaporated specimens were examined under the interference microscope. The results of this investigation do not add significant information concerning the various surface features observed under oblique illumination, since it was found that the fringe patterns were a direct consequence of the method of preparation. Although the patterns demonstrate the degree of surface roughness due to preparation scratches, various areas exhibited effects of the surface striations. These latter results are of importance because additional information is given about the observations previously made on the surfaces.

Figure 12 (a) and 12 (b) illustrate interference photographs (550 X) of samples evaporated at 900°C for 68 hours and 1080°C for 10 hours respectively. In both cases, it is evident that the fringe pattern represents surface scratches. A careful examination of these photomicrographs shows that the fringes in various areas are influenced by the oriented surface striations. In general, the overall surface roughness of a specimen evaporated at 900°C was greater than that of a specimen evaporated at 1080°C.

Grain boundary grooving was more intense at higher temperatures. This is illustrated by the photomicrograph (800 X) in Figure 13 of a grain boundary region of a specimen

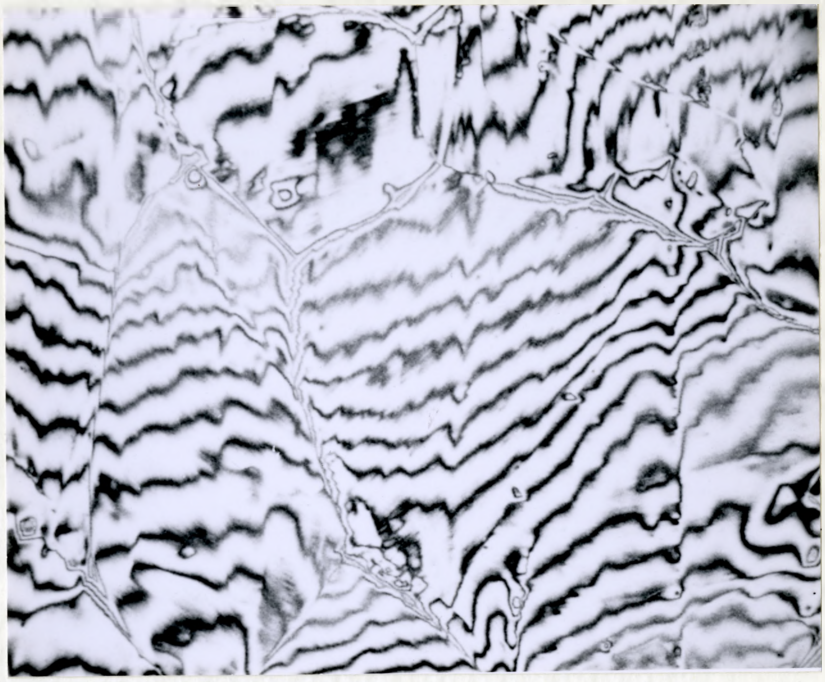

(a) Evaporated at 900°C for 68 hours

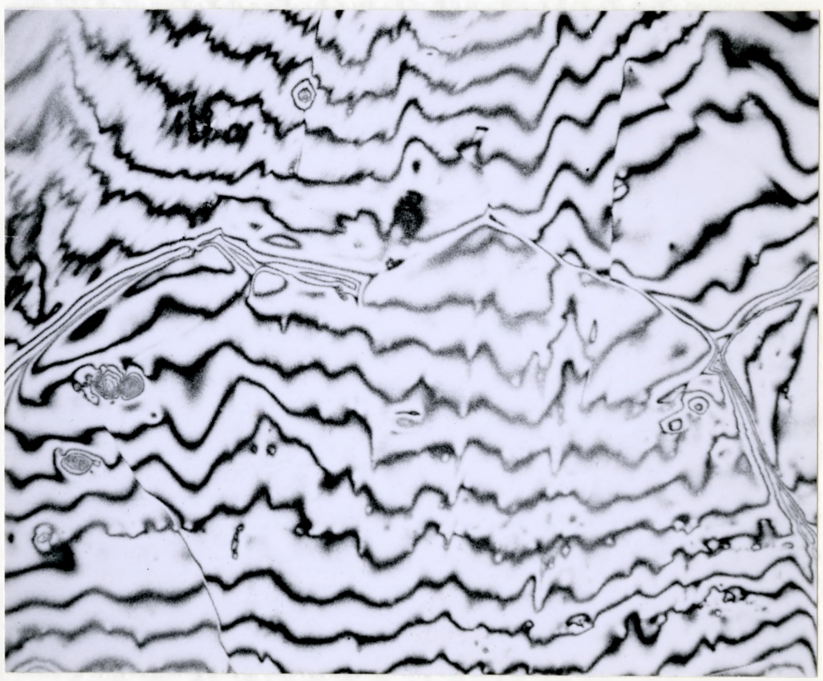

(b) Evaporated at 1080°C for 10 hours

Figure 12. Interferograms of evaporated Fe-5 percent Cr specimens; X 550.

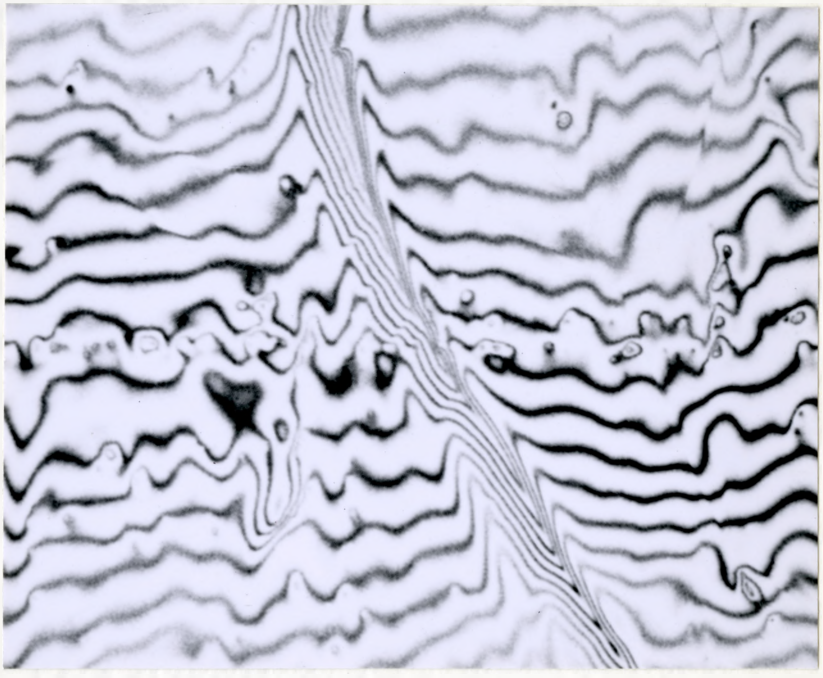

Figure 13. Interferogram of an Fe-5 percent Cr specimen evaporated at 1080°C for 10 hours; X 800.

evaporated for 10 hours at 1080°C. The depth of grooving at this temperature is appreciable and it can be readily observed that the groove profile need not be symmetric.

4.3 Evaporation of an Iron - 25 Percent Chromium Alloy in the Temperature Range 900°C to 1080°C

4.3 (i) Evaporation Kinetics

The free evaporation kinetics of the iron - 25 percent chromium alloy are summarized in Figure 14, and tabulated results are given in Table IV. As in the case of the iron - 5 percent chromium alloy, the weight loss of specimens evaporated in the investigated temperature range was directly proportional to time. Linear kinetics were obtained for experimental tests of 40 hours at 900°C and 10 hours at 1080°C. In comparison to the weight loss measurements of the iron - 5 percent chromium alloy, the rate of material loss at each temperature from the iron - 25 percent chromium alloy was approximately twice that observed for the former alloy. Again, as expected, the rate of evaporation increased with an increase in temperature.

In order to compare the vapour pressures of the iron - 25 percent chromium alloy, determined from the results of the free evaporation tests, with the equilibrium vapour pressures, determined from the results of the rates of effusion method, experiments were carried out on the iron - 25 percent chromium at 1000°C utilizing the Knudsen cell shown in Figure 4. Since the vapour pressure of the alloy at 1000°C is very small, approximately 9.0×10^{-10} atm., extremely low weight losses

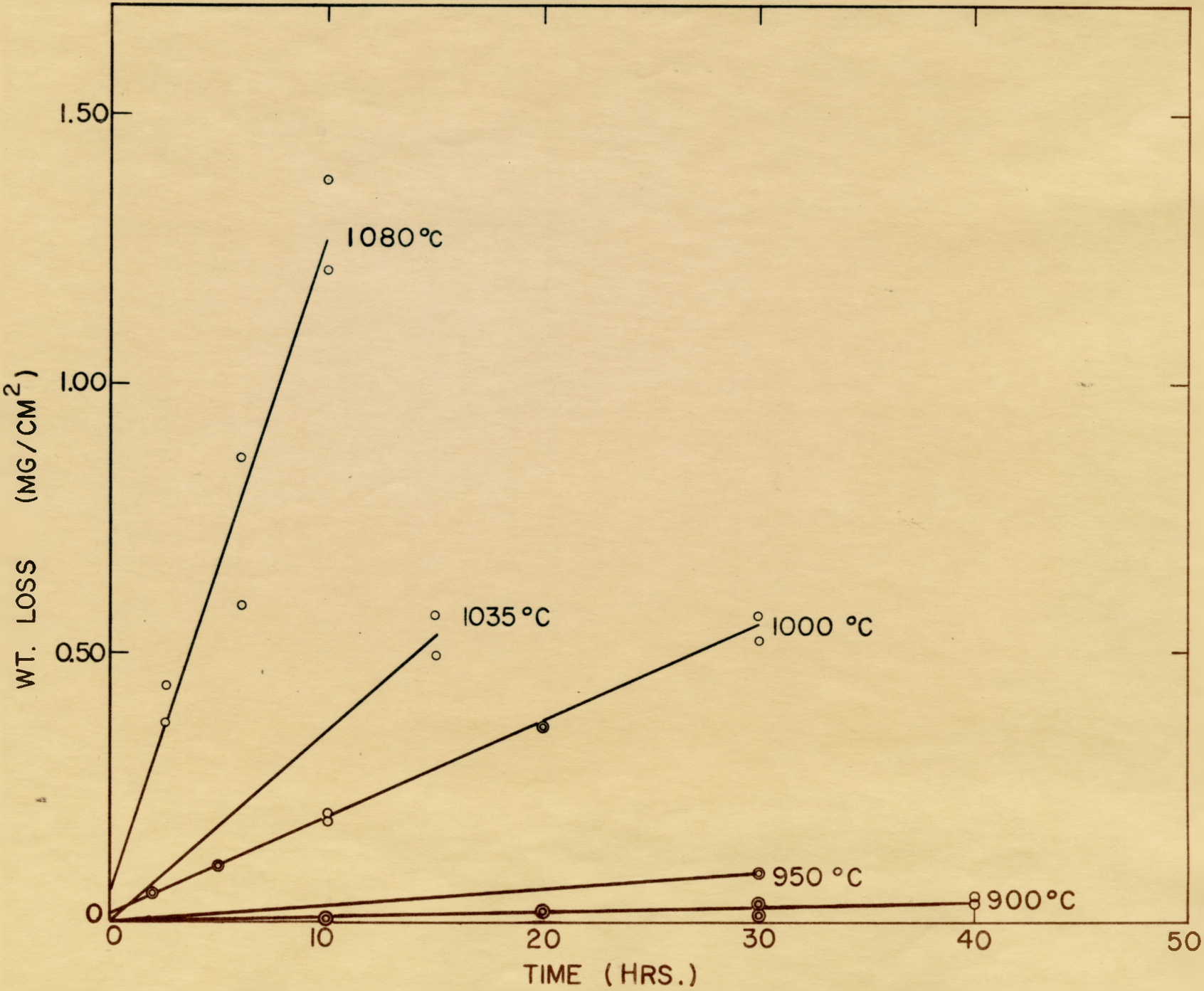

Figure 14. Free evaporation kinetics for the iron - 25 percent chromium alloy

TABLE IV

WEIGHT LOSS MEASUREMENTS / IRON - 25 PERCENT CHROMIUM ALLOY

Run Number	Temperature (°C)	Time (hrs	Weight Loss (mg/cm^2)
17a	900	10	0.006
17b	900	10	0.005
18a	900	20	0.020
18b	900	20	0.023
19a	900	30	0.028
19b	900	30	0.033
19c	900	30	0.012
19d	900	30	0.018
20a	900	40	0.044
20b	900	40	0.039
21a	950	30	0.084
21b	950	30	0.085
22a	1000	2	0.058
22b	1000	2	0.055
23a	1000	5	0.110
23b	1000	5	0.101
24a	1000	10	0.200
24b	1000	10	0.188
25a	1000	20	0.364
25b	1000	20	0.369
26a	1000	30	0.573
26b	1000	30	0.527

TABLE IV

(Cont'd)

WEIGHT LOSS MEASUREMENTS / IRON - 25 PERCENT CHROMIUM ALLOY

Run Number	Temperature (°C)	Time (hrs)	Weight Loss (mg/cm^2)
27a	1035	15	0.578
27b	1035	15	0.498
28a	1080	2.25	0.441
28b	1080	2.25	0.372
29a	1080	6	0.586
29b	1080	6	0.859
30a	1080	10	1.378
30b	1080	10	1.212

were to be expected within reasonable evaporation times. For example, assuming the iron - 25 percent chromium alloy to be ideal, the weight loss after 50 hours exposure would only be 11 μ g at 1000°C. We found that such small weight losses could not be accurately determined because oxidation of the cell body and sample material lead to spurious results for this investigation.

The results of our Knudsen cell experiments are tabulated in Table V. The non-reproducible measurements of weight losses for various times demonstrate that the method is not suitable for vapour pressure determinations of the iron - 25 percent chromium alloy in the low temperature range. It appeared that the initial large weight losses were due to vacuum degassing of the cell body and sample material. In several cases, after a series of exposures, the weight loss values approached the ideal value. However, it was noted that the cell assembly increased in weight after longer exposure times. This effect must be due to oxidation of the assembly and alloy with residual oxygen at the test temperature, and oxidation with the atmosphere at room temperature. It is emphasized that the measurements given in Table V are only tentative, since the cell assembly slowly increased in weight upon exposure to the atmosphere. The weight losses reported are the initially observed values in all cases.

TABLE V

KNUDSEN CELL MEASUREMENTS

Run Number	Cell Material	Orifice Area (cm^2)	Exposure Time (hrs)	Weight Change (ug)
1	Mo	0.0067	48	- 447
2	Mo	0.0067	51	- 1
3	Mo	0.0067	48	+ 36
4	Mo	0.0067	71	+ 387
5	pyrophyllite	0.0049	48	- 1650
6	pyrophyllite	0.0049	58.5	- 184
7	pyrophyllite	0.0049	50.5	- 7
8	Mo	0.0047	60	-42
9	Mo	0.0047	146	+ 21

4.3 (ii) Surface Topography

The features of the evaporated surfaces of the iron - 25 percent chromium specimens are illustrated by the photomicrographs taken under normal illumination (120 X) in Figures 16 (a) and 16 (b). The specimens have undergone evaporation at a 1000°C for 2 hours and 10 hours respectively. The presence of preparation scratches is obvious in both cases, however, they are not as well defined as in the case of the 5 percent chromium alloy specimens. The photomicrographs also demonstrate that the surface roughness decreases with exposure time. Grain boundary delineation is also prominent on the iron - 25 percent chromium alloy after an exposure of only 2 hours at 1000°C.

The increase in grain size with time is readily apparent on comparing Figures 16 (a) and 16 (b), and evidence of grain boundary movement is clearly illustrated by the latter photomicrograph. Since this alloy exhibits the body centred cubic structure, the absence of twinned regions on the surfaces of the evaporated specimens was, of course, expected.

In order to obtain a better understanding of grain boundary grooves and the migration of these boundaries, hot - stage microscopic techniques were adapted for the iron - 25 percent chromium alloy, under conditions of net evaporation. The photomicrographs at a magnification of 200 X in Figures 17 (a) to 17 (e) illustrate the appearance of the alloy surface, taken after exposures of 5 minutes, 3, 6, 11, and 14 hours at 900°C respectively. The appearance of boundary

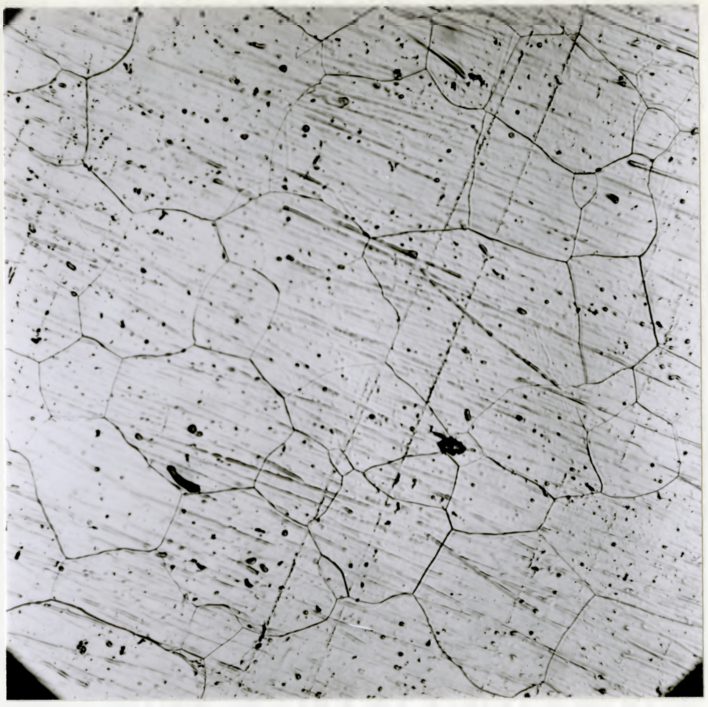

(a) Evaporated for 2 hours

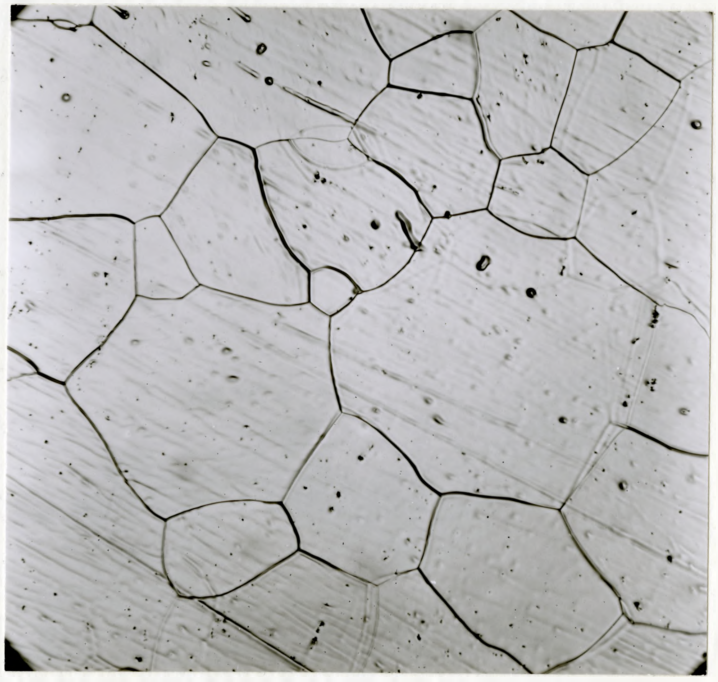

(b) Evaporated for 10 hours

Figure 16. Surface topographies of Fe-25 percent Cr specimens evaporated at 1000°C; X 120.

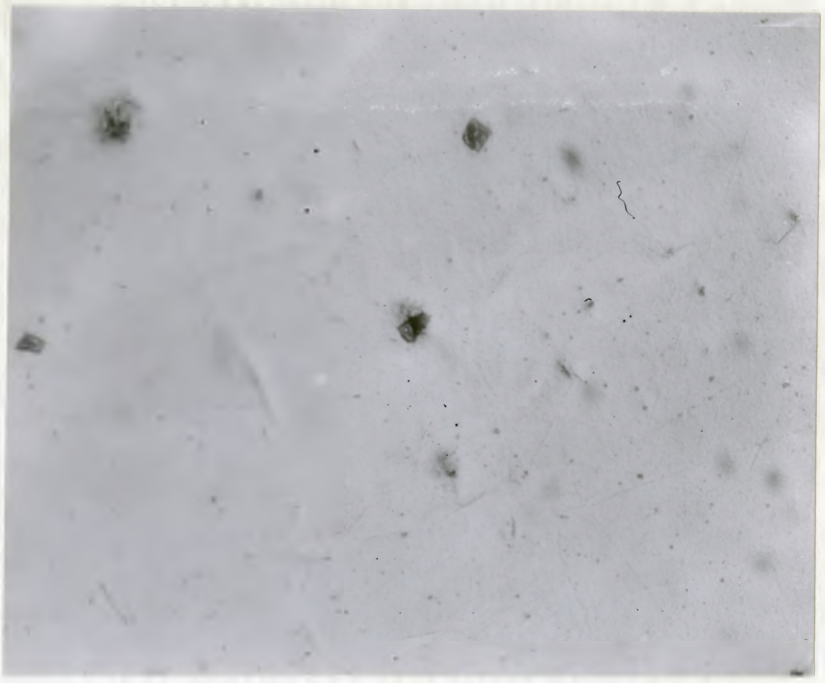

(a) Exposure time - 5 minutes

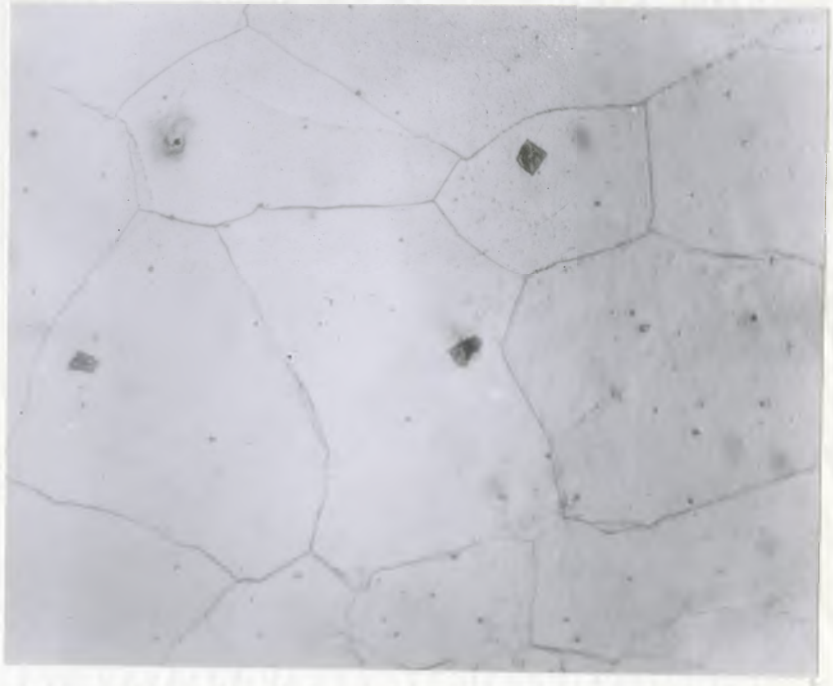

(b) Exposure time - 3 hours

Figure 17. Topographical changes in the surface of an Fe-25 percent Cr specimen evaporating at 900°C; X 200.

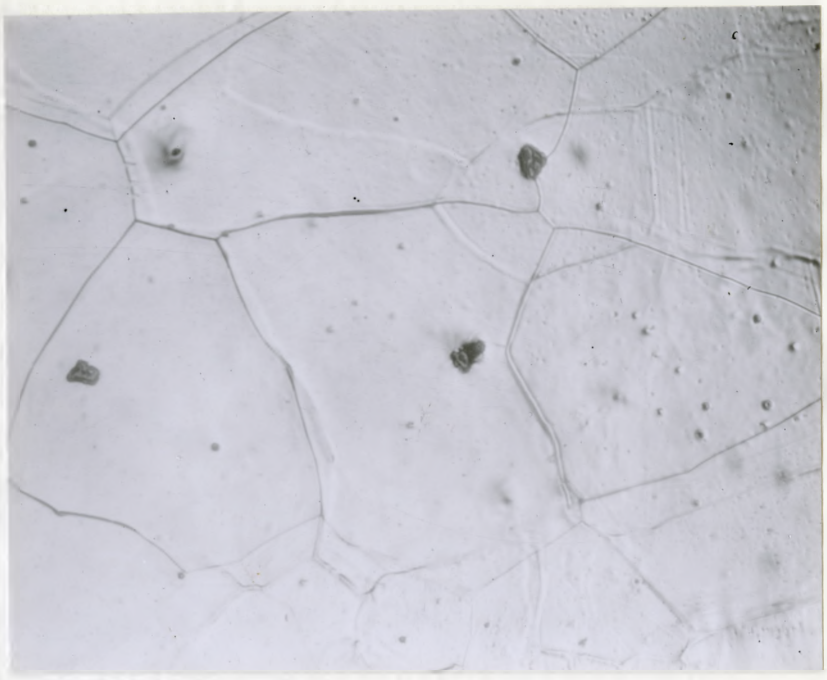

(c) Exposure time - 6 hours

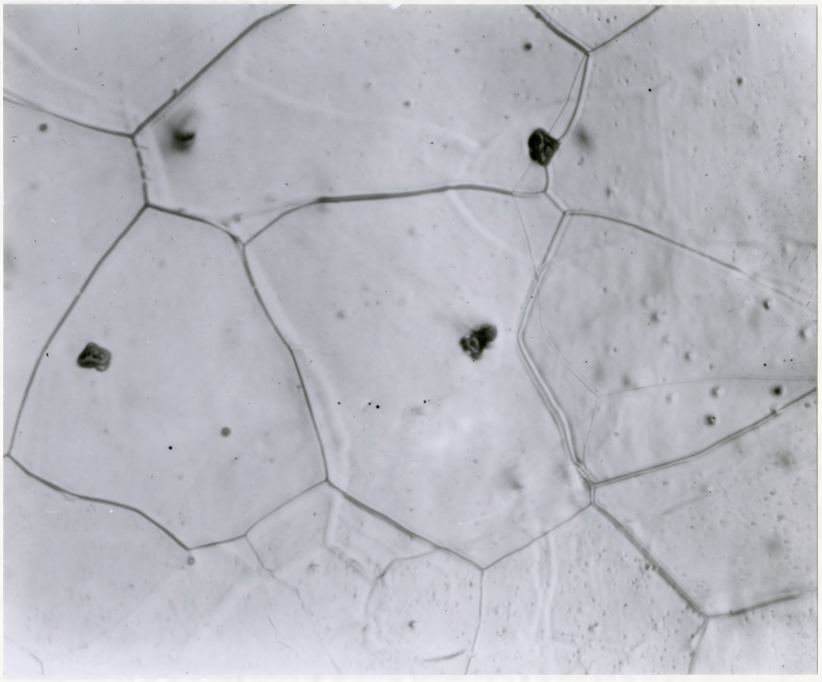

(d) Exposure time - 11 hours

Figure 17. Topographical changes in the surface of an Fe-25 percent Cr specimen evaporating at 900°C; X 200.

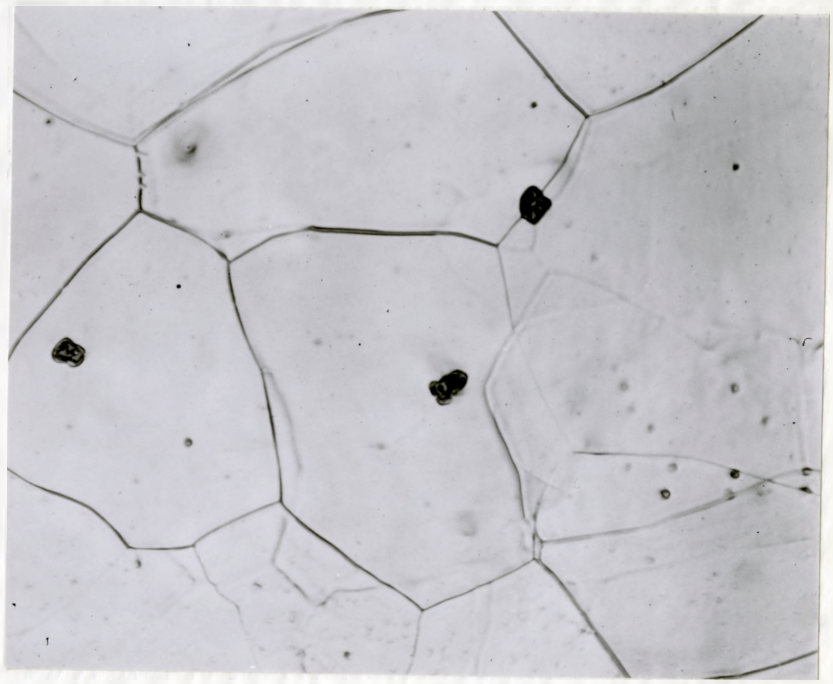

(e) Exposure time - 14 hours

Figure 17. Topographical changes in the surface of an Fe-25 percent Cr specimen evaporating at 900°C; X 200.

grooving was evident after 5 minutes at temperature, and was fully developed within 3 hours. One notes the occurrence of grain boundary migration in this sequence. Moreover, the movement of a boundary from its initial position at the surface gives rise to a "ghost" boundary, which eventually disappears by surface diffusion and evaporation. The development of the groove in the new boundary position is clearly demonstrated in Figures 17 (b) to 17 (e) inclusive.

Under oblique illumination, the fine surface features observable on the iron - 5 percent chromium alloy were not apparent. This observation was valid for the iron - 25 percent chromium alloy at all times and temperatures investigated. In every case, the specimen surfaces were completely specular in appearance. This observation is illustrated by the photomicrographs (1080 X) in Figures 18 (a) and 18 (b) of specimens evaporated at 900°C for 40 hours and at 1080°C for 10 hours respectively. These micrographs clearly demonstrate that surface striations were not observed at either the lowest or the highest investigated temperature for this alloy.

Traces of preparation scratches were visible on the specimen treated at 900°C; these were not evident on the specimen treated at 1080°C. In the latter case, the surface was specular with the exception of grain boundary grooving.

The degree of surface roughness and grain boundary grooving on this alloy may be demonstrated by reference to the interferograms of Figures 19 (a), 19 (b) and 20. Here,

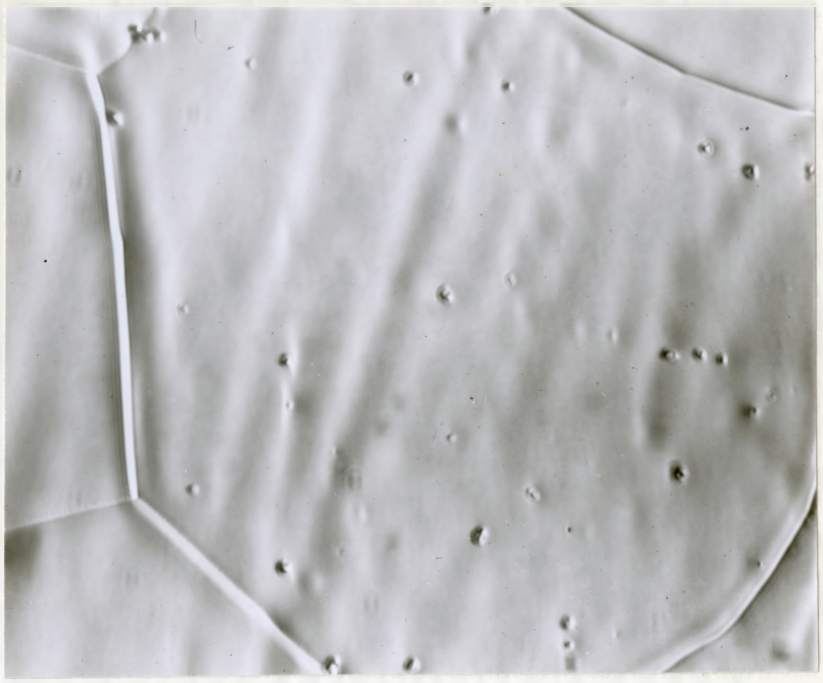

(a) Evaporated at 900°C for 40 hours

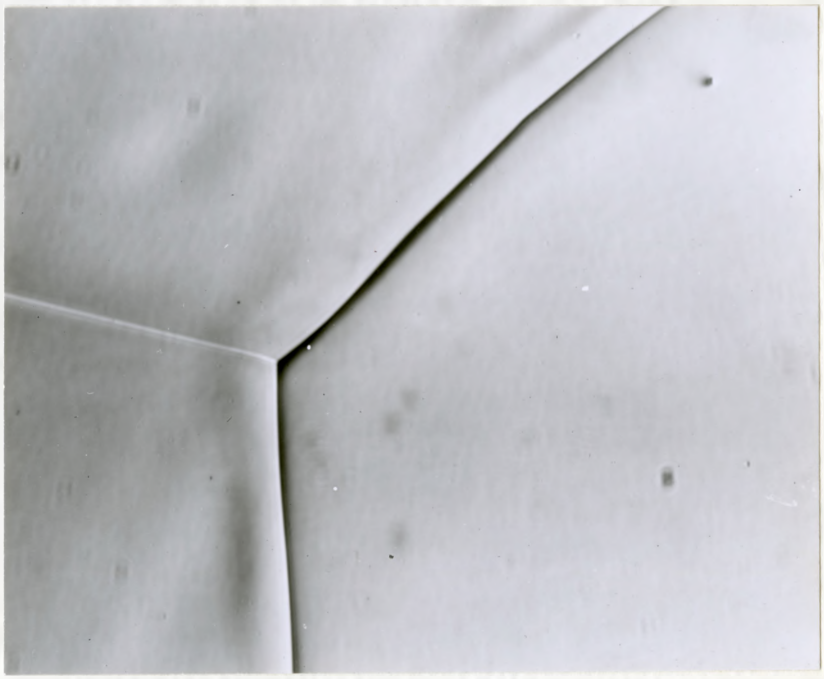

(b) Evaporated at 1080°C for 10 hours

Figure 18. Surface topographies of evaporated Fe-25 percent Cr specimens; X 1080 (oblique)

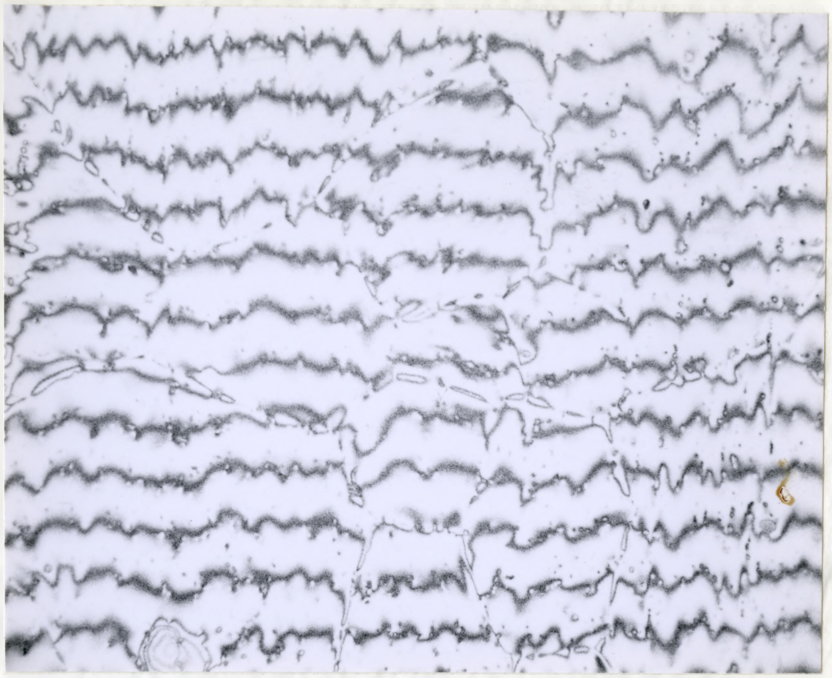

(a) Evaporated at 900°C for 20 hours

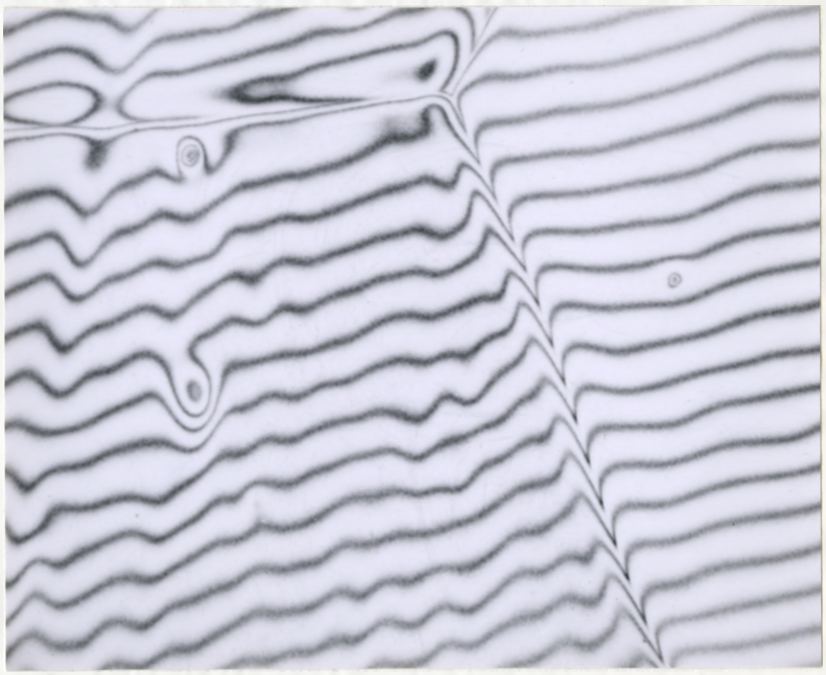

(b) Evaporated at 1080°C for 10 hours

Figure 19. Interferograms of evaporated Fe-25 percent Cr specimens; X 550.

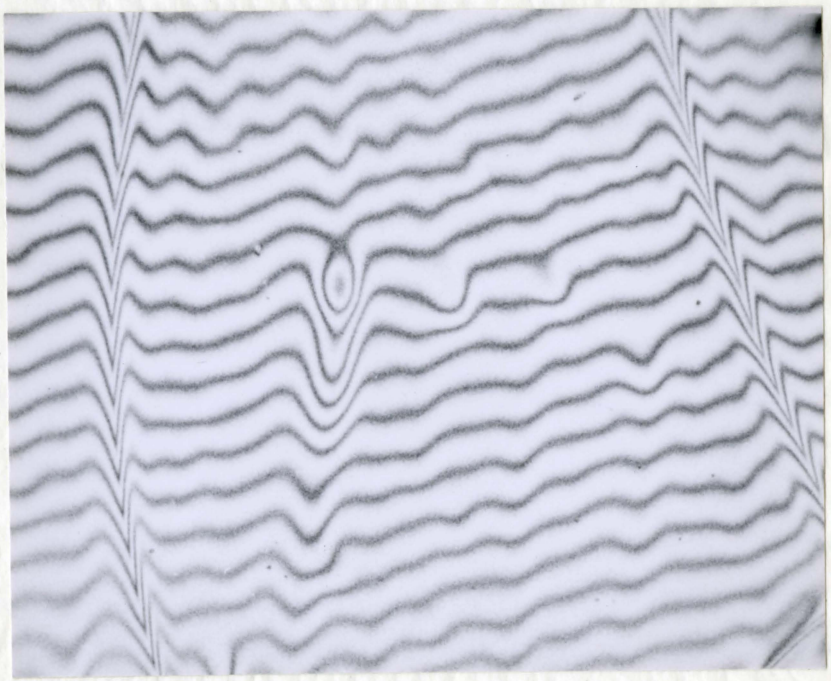

Figure 20. Interferogram of an Fe-25 percent Cr specimen evaporated at 1080°C for 10 hours; X 550.

surfaces are depicted of specimens evaporated at 900°C for 20 hours, 1080°C for 10 hours, and again, 1080°C for 10 hours, respectively. The irregular fringes demonstrate that the specimen treated at 900°C exhibits a roughened appearance due to preparation scratches. As illustrated by the more regular fringes in the photomicrographs in Figure 19 (b), this roughness effect has almost completely disappeared after exposure at 1080°C. Moreover, the duration of surface roughness from metallurgical polishing, appears to be orientation dependent. This effect is evident in Figure 19 (b), if one compares the difference of irregularities in the fringe patterns of neighboring grains. The interference fringes in the photomicrograph of Figure 20, illustrate the general profile of grain boundary grooves.

A comparison of the results from the interferometric investigations on the iron - 5 percent chromium alloy to the iron - 25 percent chromium alloy, (Figures 12 (a), (b), and 13 to Figures 19 (a), (b), and 20), illustrates the degree of surface roughness is greater on the former alloy system at all times and temperatures. Also, the depth of boundary grooving is greater on the iron - 5 percent chromium alloy after prolonged exposure at 1080°C. (Figures 13 and 20) The magnitudes of the effects shown by the interferometric microscopic studies will be discussed fully in the discussion section.

CHAPTER V

DISCUSSION

5.1 Introduction

In the following sections of this chapter, a complete analysis of the experimental results, outlined in the previous chapter, is given. The heats of evaporation and vapour pressures, calculated from the experimentally observed weight losses, are presented for both alloys considered in this investigation, and are compared to the results reported in the literature. The salient features of the evaporated alloy surfaces are discussed fully, with constant reference being made to the photographic evidence presented in the previous chapter. The condensation coefficients, determined at all temperatures for both alloys, are also presented. The significance of the values obtained for these coefficients becomes evident in the section on the mechanism of evaporation. Finally, an evaporation mechanism is proposed, based on the experimental conditions used for the determinations of the evaporation kinetics of both alloys and the results of this investigation, with reference being made to the theory of metal crystal evaporation and to pertinent data reported in the literature.

5.2 Analysis of the Weight Loss Measurements

The weight loss measurements for the iron - 5 percent chromium alloy are given in Table III and are summarized

graphically in Figure 6. In Figure 6, the weight loss in mg/cm^2 is plotted versus the time in hours for all investigated temperatures. The tests were completed in triplicate at 1000°C and in duplicate for all other temperatures. The data may be represented by linear curves for the investigated temperatures and exposure times illustrating that evaporation from this alloy proceeds at a constant rate under isothermal conditions.

The weight loss measurements for the iron - 25 percent chromium alloy are given in Table IV and are summarized graphically in Figure 14. Again, it is evident that evaporation from this alloy also proceeds at a constant rate under isothermal conditions. These rates are approximately twice those for the alloy containing 5 percent chromium. The occurrence of constant evaporation rates at all temperatures supports the viewpoint that evaporation is controlled by a surface process rather than by depletion of chromium and its diffusion in the underlying metal substrate.

The weight loss measurements were used to compute the rate constants of evaporation for both alloys at all investigated temperatures, by determining the slopes of the linear evaporation curves by the method of least squares. In order to evaluate the heats of evaporation the rate constants were expressed according to the Arrhenius equation:

$$K = Ae^{-Q/RT} \qquad (44)$$

where, K is the reaction rate constant, A is a constant, and Q is the energy or heat of activation for the process.

Arrhenius plots of these constants are shown in Figure 21. Here, the linear rate constant is the ordinate on a log scale and the reciprocal of the absolute temperature is the abscissa. The heats of evaporation were determined for both alloys from the equations of the straight lines, obtained by the method of least squares, over the temperature range 950°C to 1080°C. The values obtained for the heats of evaporation were 94.3 ± 4.5 kcal/gm. mole and 93.7 ± 6.5 kcal/gm. mole for the iron - 5 percent chromium and the iron - 25 percent chromium alloy respectively. These values for the heats of evaporation, which lie within the range of values of 99 and 94 kcal/gm. mole reported for pure iron and chromium [37] respectively, demonstrate that the temperature coefficient for alloy evaporation is determined by the escape of metal atoms from the surface to the environment.

No significance was attached in these calculations to the values of the rate constants determined at the lowest investigated temperature of 900°C. Microscopic observations illustrated that larger weight losses occurred, after short exposures, in regions markedly influenced by the method of surface preparation. It is believed that abrasion scratches act as sources of monatomic ledges during the initial stages of exposure. The presence of scratches, therefore, would give rise to an increase in the rate of evaporation. The effect of this increased rate is more important at the 900°C level, due to the normally small weight losses observed. After longer

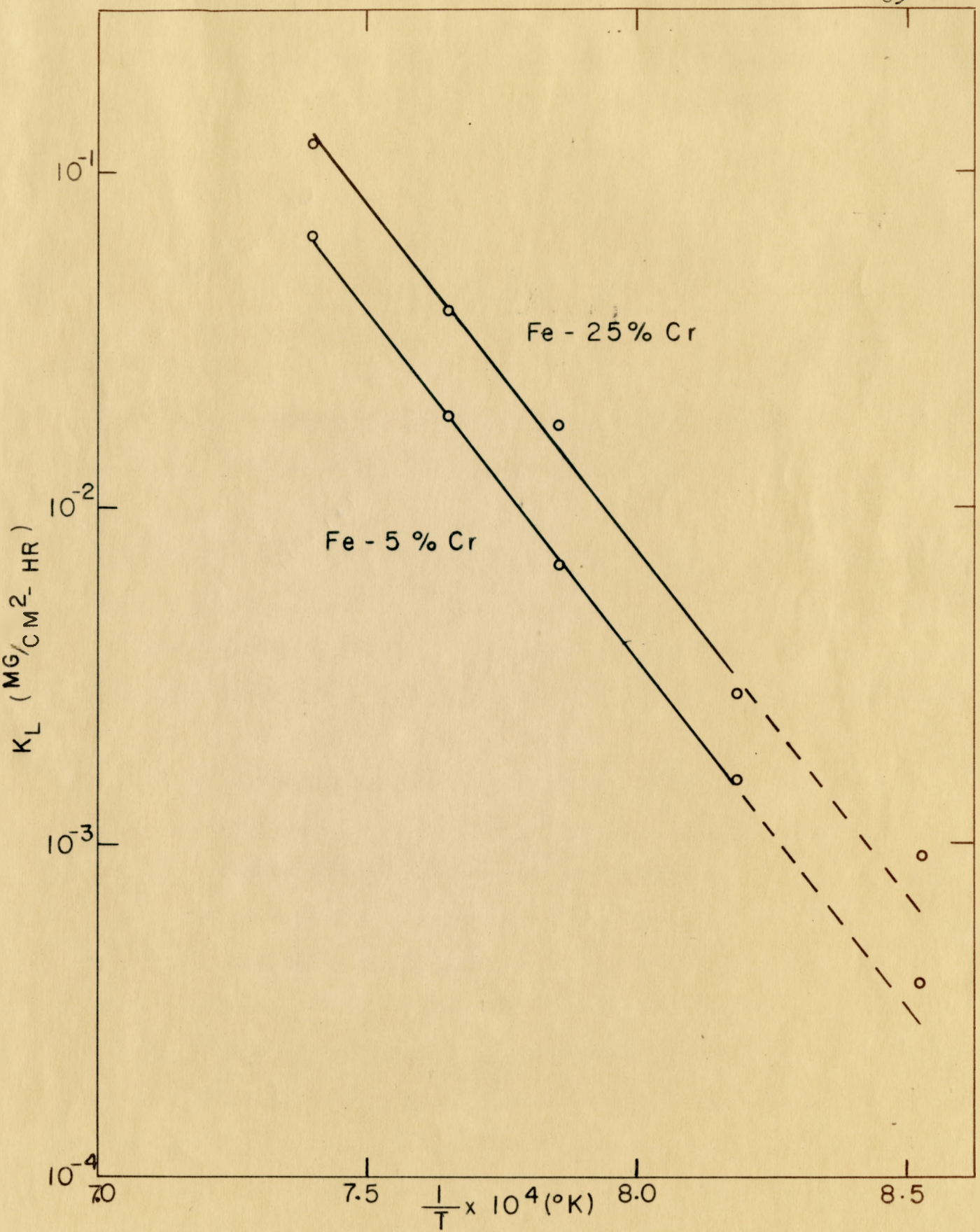

Figure 21. Arrhenius temperature coefficients of the linear evaporation constants

exposure times, these abrasion scratches disappear as evaporation proceeds, and cease to exist as sources of monatomic ledges. The presence and disappearance of abrasion scratches on the 5 percent and the 25 percent alloys are demonstrated by Figures 7 (a) and 7 (b) and Figures 16 (a) and (b) respectively.

5.3 Vapour Pressure Determinations

Using the evaporation rates computed from the weight loss measurements, the vapour pressures were calculated for the iron-5 percent and the iron-25 percent chromium alloys at the investigated temperatures from equation (6), with $\alpha = 1$ and $\sqrt{M} = \left[\frac{(M_{Cr} + M_{Fe})}{2}\right]^{\frac{1}{2}} = 7.34$. The vapour pressures determined are presented in Table VI (a) for the 5 percent chromium alloy and in Table VI (b) for the 25 percent chromium alloy.

The vapour pressures of iron - chromium alloys reported by McCabe et al.[8] and Kubaschewski et al.[41], (Knudsen method), at temperatures greater than 1200°C, are greater than the ideal pressures by a factor of approximately 1.04 for a 5 percent chromium alloy and 1.08 for a 25 percent chromium alloy. On the other hand, it may be noted that the results of Gulbransen et al.[31], who determined the vapour pressures of an iron - 21.9 percent chromium alloy at 10^{-8} mm. Hg over approximately the same temperature range investigated in this project, lie slightly lower than the vapour pressures calculated on an ideal basis.

TABLE VI

(a)

VAPOUR PRESSURES / IRON - 5 PERCENT CHROMIUM ALLOY

Temperature (°C)	Rate of Evaporation ($gm/cm^2/sec$)	Vapour pressure (atm)
900	1.08×10^{-10}	1.14×10^{-11}
950	4.27×10^{-10}	4.59×10^{-11}
1000	1.88×10^{-9}	2.05×10^{-10}
1035	5.11×10^{-9}	5.68×10^{-10}
1080	1.78×10^{-8}	2.01×10^{-9}

TABLE VI

(b)

VAPOUR PRESSURES / IRON - 25 PERCENT CHROMIUM ALLOY

Temperature (°C)	Rate of Evaporation ($gm/cm^2/sec$)	Vapour pressure (atm)
900	2.57×10^{-10}	2.70×10^{-11}
950	7.81×10^{-10}	8.39×10^{-11}
1000	4.94×10^{-9}	5.41×10^{-10}
1035	9.96×10^{-9}	1.11×10^{-9}
1080	3.36×10^{-8}	3.80×10^{-9}

The values determined in this investigation at 10^{-6} mm. Hg are also lower than the ideal values. Moreover, the vapour pressures determined at 10^{-6} mm. Hg are lower than the results of Gulbransen et al. determined at 10^{-8} mm. Hg.

5.4 Condensation Coefficient Determinations

Attempts were made to determine the vapour pressures by the Knudsen cell method, in order to compute the condensation coefficients from the relation:

$$\alpha = \frac{p_L}{p_K} \qquad (45)$$

where, p_L is the vapour pressure determined by the Langmuir method and, p_K is the vapour pressure determined by the Knudsen cell method. To this time, only tentative results are able to be reported for this investigation. However, several values reported in Table V indicate that the system iron - chromium shows some positive deviations from ideal behaviour. The results of investigations at higher temperatures,[8,41] (1250°C) demonstrate that the pressures evaluated by the Knudsen cell technique show only slight positive deviations from ideal pressures. Since pressures are not available from our Knudsen cell experiments at lower temperatures, we have calculated pressures from thermodynamic data, assuming the system iron - chromium to be ideal, and have substituted these for the Knudsen values. Thus, the condensation coefficients were calculated from:

$$\alpha = \frac{p_L}{p_{id}} \qquad (46)$$

The values determined from this ratio are reported in Table VII. For the same reasons stated in section 5.2, the values reported for the 900°C determinations were omitted in computing the average value of the condensation coefficient. The average values for the 5 percent and the 25 percent chromium alloys were found to be 0.370 ± 0.080 and 0.489 ± 0.090 respectively. In contrast, it has been shown, that the results of vapour pressure measurements on iron and chromium at higher temperatures, determined by the Langmuir and Knudsen methods, agree within the limits of experimental error. If these considerations were applicable to the iron - chromium alloys, one would expect a condensation coefficient of approximately unity.

5.5 Analysis of Surface Topographies

5.5 (i) Surface Topographies of the Iron - 25 percent Chromium Alloy

It is evident from Figures 18 (a) and 18 (b), photomicrographs of surfaces evaporated at 900°C and 1080°C, that the surface morphology of the evaporated 25 percent chromium specimens is specular at all times and temperatures investigated. The only surface irregularities evident at lower temperatures (900°C) are those due to grain boundary delineation, pitting characteristics from local regions of enhanced evaporation, and regions exhibiting traces of abrasion scratches. The effect of these scratches on specimens evaporated at lower temperatures is further illustrated by the interferogram illustrated in Figure 19 (a). At higher temperatures, the

TABLE VII

CONDENSATION COEFFICIENTS

TEMP. °C	Fe - 5 % Cr ALLOY	Fe - 25 % Cr ALLOY
900	0.438	0.468
950	0.416	0.428
1000	0.309	0.579
1035	0.448	0.494
1080	0.308	0.454
AVERAGE VALUE (950-1080)	0.370 ± 0.080	0.489 ± 0.090

surface is specular to the dimensions of at least 500 Å as shown by the constancy of fringes of the interferogram in Figure 19 (b). The depth of grain boundary grooving at higher temperatures for long exposure times is estimated to be approximately 0.25 microns from the interferograms in Figures 19.(b) and 20.

The process of grain boundary delineation is further illustrated by the hot stage photographic sequence shown in Figures 17 (a) to 17 (e) under conditions of net evaporation, at 900°C. It appears that the process is initially time dependent and approaches a steady state configuration. Grain boundary migration and the presence of "ghost" boundaries (previous boundary positions) are clearly evident. Grain boundaries are considered to act as sources of monatomic ledges which appear to migrate over the surfaces of the iron - 25 percent chromium alloy grains without giving rise to polyatomic ledge faceting.

5.5 (ii) Surface Topographies of the Iron - 5 Percent Chromium Alloy

The iron - 5 percent chromium alloy, evaporated in the austenitic state, demonstates a more complex morphology. A typical surface appearance of specimens evaporated at lower temperatures is illustrated in Figure 8. The orientation of striations and the degree of faceting are seen to be dependent on grain orientation. Moreover, the degree of faceting was observed to be temperature dependent. This is demonstrated by

Figures 10 (a) to 10 (e). The surfaces of specimens evaporated at 900°C are completely striated, whereas specimens evaporated at 1080°C for long exposure times approach a specular appearance. At 1080°C, the transition from a striated to a specular appearance occurred with time, as shown by Figures 11 (a) and 11 (b) in conjunction with Figure 10 (e).

It was also established that the striated appearance of specimens evaporated at lower temperatures could be eliminated from an austenitic specimen by a prolonged anneal at a temperature in the ferritic range. Figure 10 (f) demonstrates this effect on the surface of a specimen evaporated for 68 hours at 900°C (striated), and further evaporated for 70 hours at 840°C (specular).

The interferograms of the 5 percent chromium alloy, shown in Figures 12 (a) and 12 (b), demonstrate that the surfaces of specimens evaporated at 900°C are quite irregular and that there is a tendency to approach a specular appearance on specimens evaporated at higher temperatures. Figure 13 demonstrates that the depth of boundary grooving on specimens evaporated at higher temperatures is approximately 0.75 microns.

On comparing the surface featurs of the iron - 5 percent and the 25 percent chromium alloys, it can be seen that the surfaces of the latter specimens are specular at all times and temperatures, whereas, the 5 percent chromium specimens exhibit a transformation from a striated to a specular appearance with increasing temperature. Boundary grooving in the

case of the iron - 5 percent chromium specimens is approximately 3 times (at 0.75 microns) as great as compared to 0.25 microns for the iron - 25 percent chromium alloy. Also, striations on the iron - 5 percent chromium alloy can be eliminated by evaporation in the ferritic range. The importance of these observations will become evident when discussed in terms of the mechanism of evaporation.

5.6 Evaporation Model

In the preceding sections, it has been demonstrated that linear kinetics are obtained for relatively long exposure times illustrating that the evaporation process is surface controlled rather than by chromium depletion and its diffusion in the underlying metal substrate. The heats of evaporation, calculated from the experimental data, were approximately the same values reported for the evaporation of pure iron and chromium. This was expected on the basis that solid solutions of iron and chromium behave ideally. However, the calculated vapour pressures were lower than the Knudsen cell values expected over this temperature range. These values were also in poorer agreement with the ideal pressures than the Langmuir values reported for an iron - 21.9 percent chromium alloy over the same temperature range at 10^{-8} mm. Hg. On the basis of higher temperature data, where the Langmuir values agree with the Knudsen values, ($\alpha = 1$), one is surprised to find that the condensation coefficient is less than unity in both cases. The actual values reported were 0.370 and 0.489 for the iron - 5

percent and the 25 percent chromium alloys respectively. Even more surprising, on the basis of evaporation theory outlined in Chapter II, is the fact, that the condensation coefficient for the striated iron - 5 percent chromium alloy is less than that for the specular iron - 25 percent chromium alloy. According to evaporation theory, the reverse case should be true. However, a tentative model can be presented to explain these observations, if one takes into account the effect of chemical and physical parameters on the condensation coefficient.

We may now advance evidence to show that the condensation coefficients are, in fact, less than unity, for the conditions under which these evperiments were carried out, because of the adsorption of impurities, probably oxygen, from the residual gas. These arguments are also compatible with the morphological findings illustrated in Chapter IV. It is now more appropriate to discuss the results of Gulbransen and Andrew [31] on the vapour pressure studies of an iron - 21.9 percent chromium alloy, which readily demonstrate the effect of the residual gas pressure on the experimental results. The results of this investigation are compared to our results on the iron - 25 percent chromium alloy in Figure 22, in the form of a log p vs. 1/T plot. The ideal pressures for both alloys are also given over the same temperature range. The results of Gulbransen et al., at 10^{-8}mm. Hg, are in better agreement with the ideal values, calculated from thermodynamic data, than are those of this investigation. The condensation

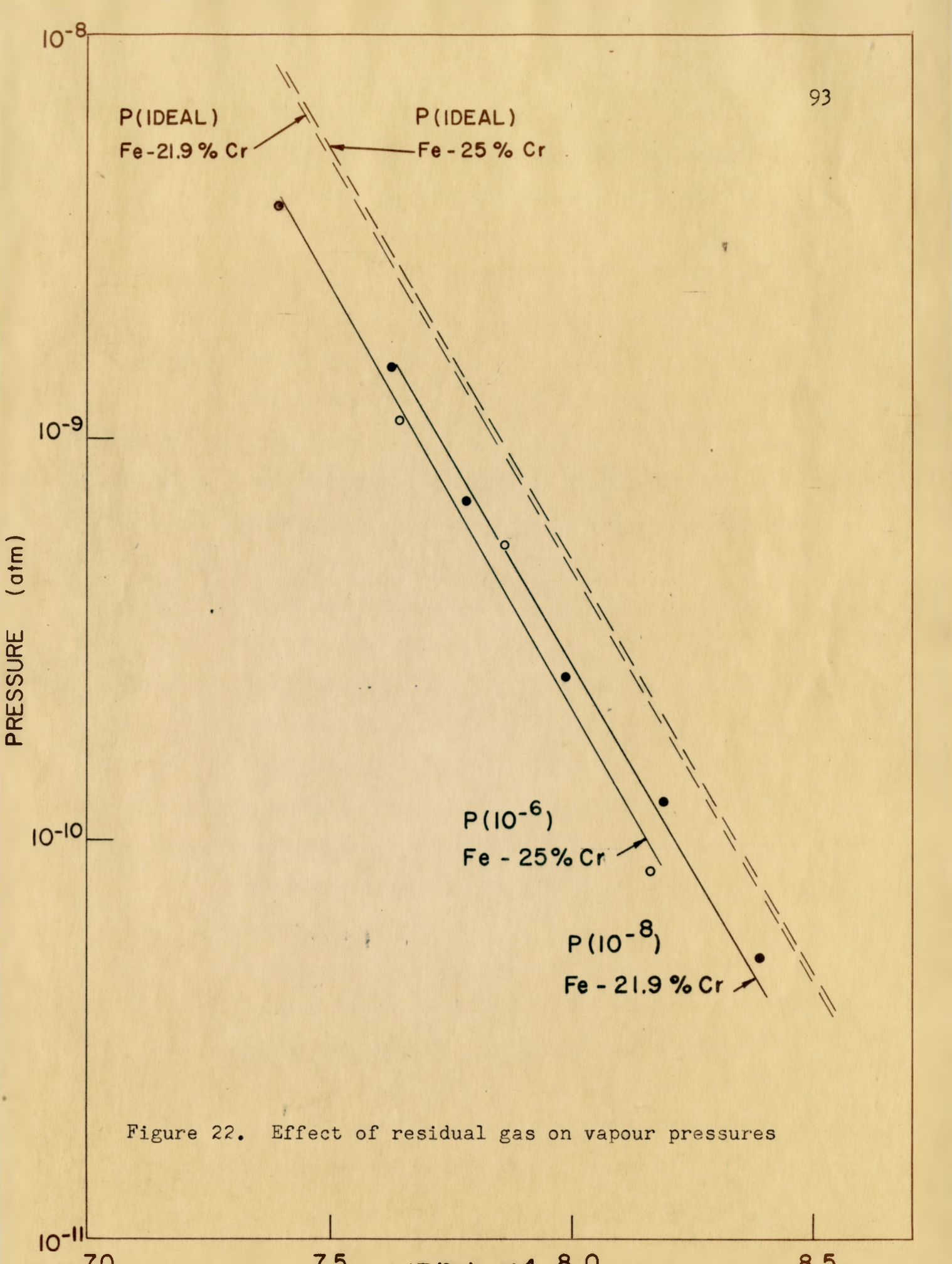

Figure 22. Effect of residual gas on vapour pressures

coefficient is in the range 0.6 to 0.7, for the residual gas pressure of 10^{-8} mm. Hg, compared to 0.4 to 0.5 for evaporation at 10^{-6} mm. Hg. These results suggest that the condensation coefficient for polycrystalline alloys would approximate unity, as for high temperature measurements, if surface contamination could be avoided.

In the discussion on the chemical properties affecting the condensation coefficient, section 2.4 (vi), reference was made to the findings of Bènard et al.[32], that the occurrence of a striated or a specular surface on iron and iron - chromium alloys was dependent on the degree of oxygen adsorption. At oxygen pressures less than the dissociation pressure of the most stable oxide, (Cr_2O_3, 1.0×10^{-22} atm. at 1000°C)[37] selective adsorption of oxygen could occur on the different crystalline faces. For a minimization of surface energy, a non-planar striated surface could arise, if the adsorption of oxygen is sufficient, and if the temperature is high enough to permit the surface to redistribute itself by surface diffusion or some other process. In agreement with this viewpoint, these investigators demonstrated that specular surfaces are obtained, when oxygen is rigorously removed from the system. The transformation from a striated to a specular surface occurred at a critical oxygen potential as determined by H_2O/H_2 ratios at a specific temperature. This critical range existed in both the austenitic and ferritic range, the critical curve being continuous at the transformation temperature.

The evaporating conditions in this investigation, at a residual gas pressure of 10^{-6}mm. Hg, are such, that these requirements for selective oxygen adsorption prevail. In the case of the iron - 25 percent chromium alloy, oxygen adsorption must not be sufficient in any case. For the iron - 5 percent chromium alloy, the oxygen pressure must be sufficient to promote striated surfaces at 900°C. On the other hand, at higher temperatures, oxygen adsorption must play a minor role, since the striations were not as prominent and tended to disappear with time. This also appeared to be the case, if the alloys initially evaporated in the austenitic state, were re-evaporated in the ferritic range.

There are essentially two ways in which oxygen can be removed from the surface of the iron - 25 percent chromium alloy. These are illustrated diagrammatically in the top portion of Figure 23. In the first case, evaporating metal could getter residual oxygen, possibly form some molecular oxide, and deposit on the cooler sections of the furnace assembly. The ratio of chromium evaporation from the alloy containing iron - 25 percent chromium to that of the iron - 5 percent chromium alloy is approximately 10. In the second case, oxygen could be removed from the surface by its diffusion into the metal substrate. The ratio of the oxygen diffusion constants [43] for the alloy in the ferritic and austenitic states is approximately 10^2. The latter process would be the predominant mechanism for oxygen removal from the

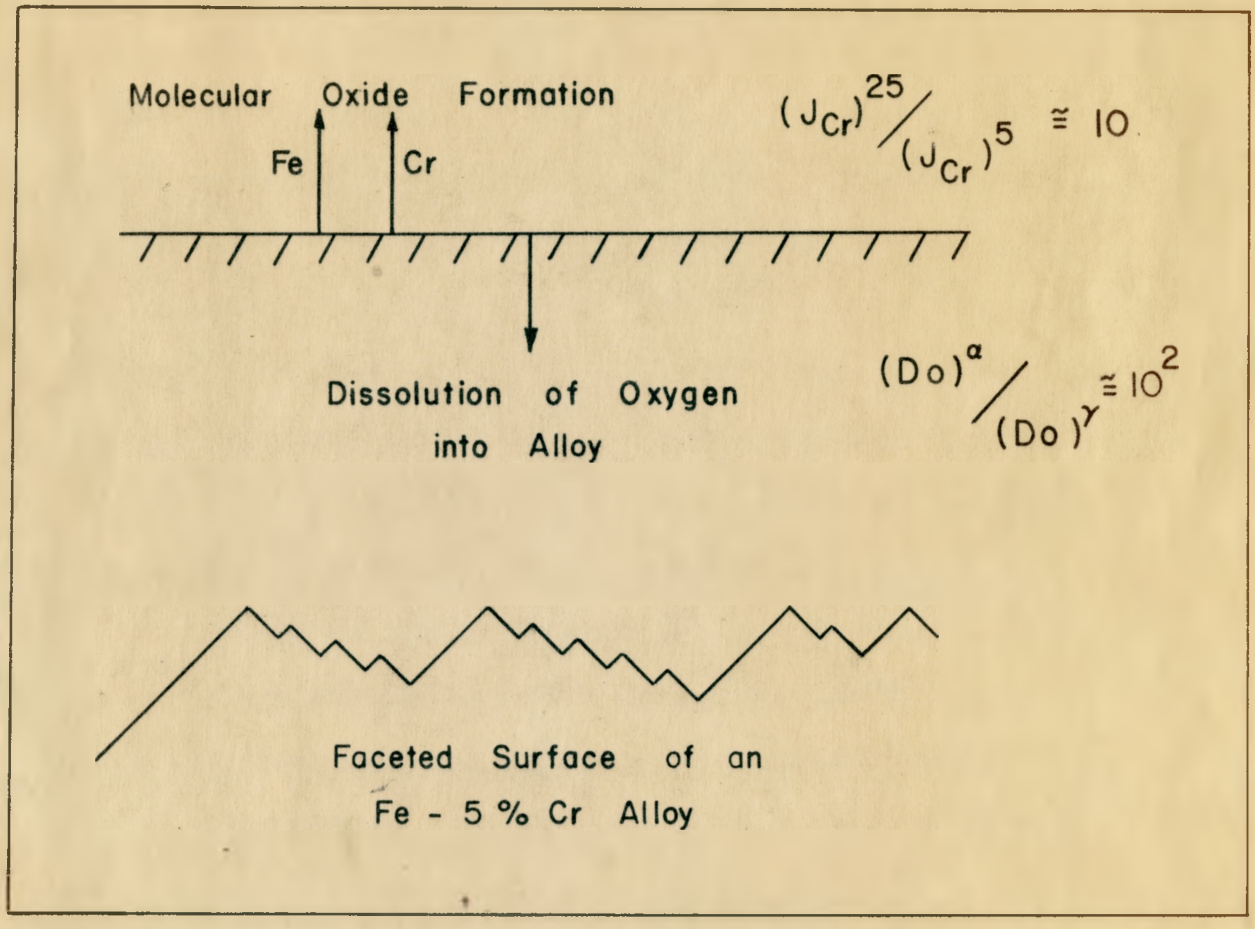

Figure 23. Evaporation model

iron - 5 percent chromium alloy specimen re-evaporated in the ferritic range at 840°C. All conditions are such, that evaporation is occurring under a smaller degree of oxygen adsorption on the iron - 25 percent chromium alloy and the 5 percent alloy in the ferritic state as our metallographic observations have illustrated in the range of specular surface formation.

In the case of the iron - 5 percent chromium alloy at higher temperatures, the rate of evaporation and the rate of oxygen solution are sufficient to promote specular surface formation. On the other hand, at lower temperatures, the selective adsorption of oxygen on different crystalline faces would be larger under these evaporating conditions. Here, the surface is faceted giving rise to a topography as shown in the bottom portion of Figure 23. The non-planar morphology is stabalized by selective oxygen adsorption.

If it is assumed, that the evaporation process occurs by the ledge mechanism outlined in Chapter II, oxygen adsorption must decrease the motion of monatomic ledges (poisoning) during evaporation. This viewpoint is supported by the fact that the condensation coefficient for the iron - 5 percent chromium alloy, evaporating under conditions of greater oxygen adsorption, is of smaller magnitude than that of the iron - 25 percent chromium alloy. Slight oxygen adsorption on the surface of the iron - 25 percent chromium alloy at ledge positions could account for the decrease in the condensation coefficient from 1 to 0.5.

This explanation must be tentatively accepted until accurate Knudsen cell measurements of vapour pressures, or chemical activities of iron and chromium in the system iron - chromium, have been determined. It is still possible that metal is evaporating from the specular surface of the iron - 25 percent chromium alloy from monatomic ledges, under ideal conditions, in which case, the condensation coefficient would be expected to be much less than unity, and approximate a value of 1/3, as is indicated by the theory of evaporation.

CONCLUSIONS

As a result of the investigations carried out on the iron - 5 percent chromium and the iron - 25 percent chromium alloys in the temperature range 900°C to 1080°C, the following conclusions may be presented:

1. Linear evaporation rates were observed for both alloys at all investigated temperatures, which demonstrate that the evaporation is controlled by a surface reaction.

2. The values for the heats of evaporation are within the range of values reported for pure iron and chromium, illustrating that the temperature coefficient of alloy evaporation is determined by the escape of metal atoms from the surface to the environment.

3. The vapour pressures of both alloys, calculated by means of the Langmuir equation for free evaporation, are lower than the ideal pressures, as a result of the invalid assumption that the condensation coefficient is unity for the iron - chromium system over the investigated temperature range.

4. The occurrence of a striated or specular surface topography is dependent on the degree of selective impurity adsorption, probably oxygen, from the residual gas in the evaporation chamber.

5. The condensation coefficients for an iron - 5 percent and an iron - 25 percent chromium alloy are in the range

0.4 to 0.5, for evaporation between 900°C and 1080°C in a vacuum of 10^{-6} mm. Hg, in contrast to a value of unity for pure iron and chromium at higher temperatures.

6. Evaporation from the surface of the iron - 5 percent chromium alloy is occurring under a greater degree of selective impurity adsorption as compared to evaporation from the surface of the iron - 25 percent chromium alloy.

7. The possibility exists, that evaporation is occurring from the iron - 25 percent alloy specimens under conditions outlined by the theory of metal evaporation, in which case, the condensation coefficient is expected to approach a value of 1/3.

APPENDIX

CHEMICAL COMPOSITION OF IRON - CHROMIUM ALLOYS

Iron - 5 Percent Alloy

C	P	Si	Mn	S	Cr	Fe
0.00	0.005	0.019	0.04	0.007	5.0	balance

Iron - 25 Percent Alloy

C	P	Si	Mn	S	Cr	Fe
0.00	0.017	0.053	0.20	0.015	25.0	balance

BIBLIOGRAPHY

1. J.M. Perrow, Master's Thesis, McMaster University, Hamilton, Ont. (1961)

2. R. Speiser and J.W. Spretnak, Vacuum Metallurgy (Electrochemical Soc., Boston, 1955), p.155

3. I. Langmuir, Phys. Rev. 2, 329 (1913)

4. M. Knudsen, Ann. Physik. (Leipzig) 29, 179 (1909); Kinetic Theory of Gases, Meuthen Ltd., (1934)

5. M. Knudsen, Ann. Physik. 28, 75 (1909)

6. P. Clausing, Ann. Phys. 12, 961 (1932)

7. E.H. Kennard, Kinetic Theory of Gases, McGraw-Hill Book Co., N.Y. (1938) p.307

8. C.L. McCabe, R.G. Hudson, and H.W. Paxton, A.I.M.E. Trans. 212, 102 (1958)

9. O. Knacke and I.N. Stranski, Progress in Metal Physics, Vol. 6, Pergamon Press Ltd. London (1956)

10. H.L. Johnston and A.L. Marshall, J. Am. Chem. Soc. 62, 1382 (1940)

11. R.B. Holden, R. Speiser, and H.L. Johnston, ibid, 70, 3897 (1948)

12. G. Wessel, Z. Physik. 130, 539 (1951)

13. Ko, J. Franklin Inst. 217, 173 (1934)

14. J.P. Hirth and G.M. Pound, A.I.M.E. Trans. 215, 932 (1959)

15. J.P. Hirth and G.M. Pound, J. Chem. Phys. 26, 1216 (1957)

16. J.P. Hirth and G.M. Pound, Acta Met. 5, 649 (1957)

17. M. Polyani and E. Wigner, Z. Physik. Chem. 139A, 439 (1928)

18. K. Neumann, ibid, 196, 16 (1950)

19. W. Kossel, in Falkenhagen, Quantentheorie und Chemie, Vortrag, Leipzig, (1928); Naturwissenschaften, 18, 901 (1930); Ann. Phys. 33, 651 (1938)

20. M. Volmer, Kinetic der Phasenbildung, Dresden and Leipzig (1939)

21. W.K. Burton and N. Cabrera, Disc. Faraday Soc. 5, 33 (1949)
W.K. Burton and F.C. Frank, Nature Land. 163, 398 (1949); Phil Trans. Roy. Soc. (A) 243, 299 (1951)

22. F.C. Frank, Disc. Faraday Soc. 5, 67 (1949)

23. O. Knacke, I.N. Stranski, and G. Wolff, Z. Electrochem. 56, 476 (1952)

24. O. Knacke, I.N. Stranski, and G. Wolff, Z. Phys. Chem. 198, 157 (1951); Zur Struktur und Materie der Festkörper, Springer (1952), p.34

25. I. Langmuir, Phys. Rev. 8, 149 (1916)

26. M. Knudsen, Ann. Phys. (Leipzig) 28, 75 (1908); 35, 389 (1911)

27. M. Volmer and I. Estermann, Z. Phys. 7, 13 (1921)

28. I.N. Stranski, Z. Phys. Chem. 136, 259 (1928); (B) 11, 421 (1931)
I.N. Stranski and R. Kaischew, Z. Krist. 78, 373 (1931)

29. O. Knacke and I.N. Stranski, Ergebnisse d. exakt. Naturwiss. 26, 383 (1952)

30. J.P. Hirth and G.M. Pound, Acta Met. 5, 649 (1957)

31. E.A. Gulbransen and KF. Andrew, A.I.M.E. Trans. 221, 1247 (1961)

32. J. Bènard and J. Moreau, Acta Met. 10, 247 (1962)

33. E.D. Hondros and A.J.W. Moore, Acta Met. 8, 647 (1960)

34. H.A. Jones, I. Langmuir, and G.M.J. MacKay, Phys. Rev. 30, 201 (1927)

35. A.L. Marshall, R.W. Dornte, and F.J. Norton, J. Am. Chem. Soc. 59, 1161 (1937)

36. J.W. Edwards, H.L. Johnston, and W.E. Ditmars, ibid, 73, 4729 (1951)

37. J.F. Elliott and M. Gleiser, Thermochemistry for Steelmaking, Vol. I, Addison - Wesley Publishing Co., Reading, Mass. (1960) p.214, 266

38. J.P. Morris, G.R. Zellars, S.L. Payne, and R.L. Kipp, U.S. Bur. of Mines, Report of Investigation 5364 (September, 1957)

39. E. Bauer and R. Brunner, Helv. Chem. Acta 17, 958 (1934)

40. R. Speiser, H.L. Johnston, and P. Blackburn, J. Am. Chem. Soc. 72, 4142 (1950)

41. O. Kubaschewski and G. Heymer, Acta Met. 8, 416 (1960)

42. Metals Handbook, The American Society for Metals, Cleveland, Ohio, (1948), p.1194

43. H. Schenck, E. Schmidtmann, and H. Müller, Arch. Eisenhuttenwes. 31, 121 (1960)